NATIONAL AERONAUTICS AND SPACE ADMINISTRATION

MSC INTERNAL NOTE NO. 68-FM-50

February 23, 1968

NAVIGATION AND GUIDANCE SYSTEMS PERFORMANCE FOR MANNED MISSIONS TO VENUS AND MARS BETWEEN 1972 AND 1980

By Flora B. Lowes
and
Thomas B. Murtagh,
Advanced Mission Design Branch

MISSION PLANNING AND ANALYSIS DIVISION

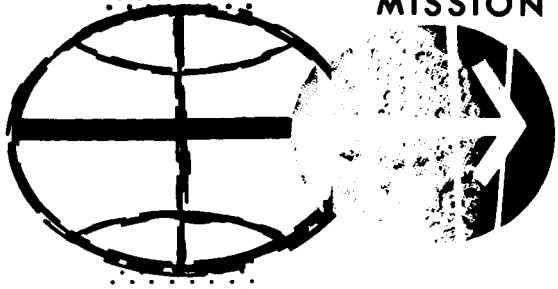

MANNED SPACECRAFT CENTER
HOUSTON, TEXAS

MSC INTERNAL NOTE NO. 68-FM-50

NAVIGATION AND GUIDANCE SYSTEMS PERFORMANCE FOR MANNED MISSIONS TO VENUS AND MARS BETWEEN 1972 AND 1980

By Flora B. Lowes and Thomas B. Murtagh
Advanced Mission Design Branch

February 23, 1968

MISSION PLANNING AND ANALYSIS DIVISION
NATIONAL AERONAUTICS AND SPACE ADMINISTRATION
MANNED SPACECRAFT CENTER
HOUSTON, TEXAS

Approved: Jack Funk
Jack Funk, Chief
Advanced Mission Design Branch

Approved:
John P. Mayer, Chief
Mission Planning and Analysis Division

TABLES

CONTENTS

FIGURES

NAVIGATION AND GUIDANCE SYSTEMS PERFORMANCE FOR MANNED MISSIONS TO VENUS AND MARS BETWEEN 1972 AND 1980

By Flora B. Lowes and Thomas B. Murtagh

SUMMARY

Navigation and guidance analyses for a 1972 Venus flyby, a 1975 Mars flyby, and a 1977 Mars stopover were made using state-of-the-art techniques. This study includes analyses for all phases of each mission; performance evaluations for both the manned spacecraft and the unmanned probe are included for each outbound phase.

The midcourse navigation system includes both Earth-based radar and onboard tracking capabilities for updating position and velocity estimates of the spacecraft or probe using a Kalman filter. The guidance system utilizes both fixed- and variable-time-of-arrival guidance for computing the velocity corrections and appropriate target dispersions.

Excluding the fuel cost for maneuvers in the orbital phase of the Mars stopover mission, the results of the study indicate that a total midcourse ΔV for each mission is about 200 fps (1σ); resulting spacecraft delivery accuracies are 4 n. mi. at Mars or Venus for the outbound phase and 1 n. mi. at Earth for the return phase. Similarly, for the probe delivery, an accuracy somewhat less than 5 n. mi. can be obtained at the cost of one correction of approximately 80 fps (1σ). These results would apply to other interplanetary missions with similar characteristics.

INTRODUCTION

Assuming that the planets of primary scientific interest for manned interplanetary missions are Venus and Mars, the reference missions chosen for evaluating navigation and guidance systems performance were a 1972 Venus flyby, a 1975 Mars flyby, and a 1977 Mars stopover. These missions, which are within the limits of present technology, are representative of any which might be considered for the time period 1972 to 1980.

For the analysis, all navigation types and schedules were the same for each mission in order to directly compare obtainable accuracies and fuel costs. A combination of Earth-based radar tracking and onboard sextant measurements was assumed for the navigation of the spacecraft; a radar system onboard the spacecraft tracked the probe during the probe delivery phase of each mission. For the Earth-based radar observations, the tracking stations were Goldstone, Johannesburg, and Woomera; the viewing station measured range and range-rate simultaneously. These radar data are corrupted by a variety of errors but this analysis considers only the white noise errors.

The onboard sextant error model considers the sum of three error sources, assumed uncorrelated with respect to each other and from one observation to the next. The first error is the basic instrument error, the second is an error in the knowledge of the observed body radius, and the third is due to the uncertainty in the position of the observed body.

The navigational measurements made at specified intervals during the mission were processed in turn by a Kalman filter. The spacecraft onboard radar system tracking the probe measured the relative range and range-rate between the manned spacecraft and the unmanned probe. An augmented Kalman filter was used to simultaneously process probe and spacecraft tracking data after probe separation during the outbound phase.

The velocity correction execution error was assumed to be a function of random errors in engine cutoff and in thrust vector orientation and magnitude. The midcourse velocity corrections were computed using both fixed- and variable-time-of-arrival guidance. The fixed-time-of-arrival (FTA) guidance law attempts to null all components of the position vector error at the nominal time of arrival at the target; the variable-time-of-arrival (VTA) guidance law nulls the radius and track components of position error while minimizing the magnitude of the commanded correction. For this study, VTA guidance was used inside the sphere of influence (SOI) of the target planet; FTA guidance was used elsewhere. It has been found that best results are obtained from combined use of these two guidance laws. These corrections are influenced by the navigation system accuracy, type and number of navigation measurements processed, and sighting body diameter and ephemeris errors.

The midcourse velocity correction schedules were nonoptimum but were selected to produce RMS periapsis radius dispersions less than 5 n. mi. at the target planet. The nominal navigation and guidance system errors are listed in table I. Discussions of the Earth-based radar and onboard sextant error models can be found in references 1, 2, and 3.

The total trip times of the missions are 370 days for the Venus flyby, 672 days for the Mars flyby, and 980 days - including 300 days orbital staytime - for the Mars stopover. The Earth injection and the Earth return velocities for each mission are within the capability of the uprated Apollo systems.

The unmanned probe reference trajectory of each mission is computed assuming that the probe is separated from the manned spacecraft at the Venus or Mars SOI. The inclination of the probe trajectory was equal to that of the spacecraft. The probe lead or lag time with respect to spacecraft arrival at the approaching planet periapsis, entry altitude, speed, and flight-path angle are calculated as a function of probe-spacecraft separation ΔV.

SYMBOLS

$A(t)$	sensitivity vector which relates star-planet-horizon angle deviations to state vector deviations
$B(t)$	sensitivity matrix which relates relative range and range-rate deviations to state vector deviations
$E(t)$	uncertainty covariance matrix
$E_p(t)$	probe uncertainty covariance matrix
$E_s(t)$	spacecraft uncertainty covariance matrix
$H(t)$	sensitivity matrix defined by equation (A8)
I	identity matrix of appropriate dimensions
$K(t)$	weighting matrix defined in equations (A13)
$M(t)$	3×3 matrix defined in equations (A13)
$P(t)$	augmented uncertainty covariance matrix defined by equation (A5)
$R(t)$	covariance matrix of measurement errors defined by equation (A14)
r_B	target planet radius
$\bar{r}_p$	unmanned probe position vector with respect to target planet
$\bar{r}_s$	spacecraft position vector with respect to target planet

r_s	magnitude of spacecraft position vector
t_o, t	arbitrary initial and final times, respectively
$\hat{u}_s$	unit vector to star
$\bar{V}_p$	unmanned probe velocity vector with respect to target planet
$\bar{V}_s$	spacecraft velocity vector with respect to target planet
$\bar{V}_\rho$	relative velocity vector of unmanned probe with respect to spacecraft ($\bar{V}_\rho = \bar{V}_p - \bar{V}_s$)
$X(t)$	dispersion covariance matrix
β	angle between a star and the target planet horizon line of sight
$\Gamma(t,t_o)$	6×6 unmanned probe state transition matrix
$\delta(\ )$	small deviation of ( )
$\Delta E(t)$	change to uncertainty covariance matrix as result of a navigation measurement or a guidance maneuver
$\Delta X(t)$	change to dispersion covariance matrix as result of a guidance maneuver
θ	one-half the target planet disc subtended angle ($\sin\theta = r_B/r_s$)
$\Theta(t,t_o)$	12×12 augmented state transition matrix defined by equation (A3)
$\xi(t)$	augmented state vector deviation defined by equation (A2)
$\bar{\rho}$	relative position vector of unmanned probe with respect to spacecraft ($\bar{\rho} = \bar{r}_p - \bar{r}_s$)
ρ	magnitude of relative position vector (range)
$\dot{\rho}$	probe-spacecraft relative range-rate ($\dot{\rho} = \frac{\bar{\rho}}{\rho} \cdot \bar{V}_\rho$)
σ_β^2	variance of star-horizon observable
σ_ρ^2	onboard radar range variance
$\sigma_{\dot{\rho}}^2$	onboard radar range-rate variance

$\Phi(t,t_o)$ 6 × 6 spacecraft state transition matrix

Superscripts

$( )^+$ ( ) after navigation measurement or guidance maneuver

$( )^-$ ( ) before navigation measurement or guidance maneuver

$( )^{-1}$ inverse of ( )

$( )^T$ transpose of ( )

ANALYSIS

Trajectory Characteristics

The missions considered for this study were a 1972 Venus flyby, a 1975 Mars flyby, and a 1977 Mars stopover. The reference trajectories were calculated using matched-conic techniques (ref. 4), and the state transition matrices used to propagate the errors were derived analytically for two-body conic trajectories. The reference trajectory characteristics are summarized in table II. The stopover orbital parameters for the 1977 Mars mission are presented in table III. Further discussion of this stopover orbit can be found in reference 5. The projections of these trajectories in the ecliptic plane are illustrated in figure 1.

Navigation and Guidance System Equations

The pertinent error matrices usually referred to in navigation and guidance system analyses are the uncertainty covariance matrix, $E(t)$, and the dispersion covariance matrix, $X(t)$. The uncertainty matrix is a measure of how far the estimated trajectory is from the actual trajectory; the dispersion matrix represents the deviation of the actual trajectory from the nominal. The linearized error analysis equations used to update $E(t)$ and $X(t)$ as a result of a navigation measurement or a guidance maneuver are discussed in references 1, 2, 3, and 6 and can be written in a generalized form as

$$E(t) = \Phi(t,t_o)\, E(t_o)\Phi^T(t,t_o) + \Delta E(t) \qquad (1)$$

and

$$X(t) = \Phi(t,t_o)\, X(t_o)\Phi^T(t,t_o) + \Delta X(t) \qquad (2)$$

where $\Phi(t,t_o)$ is the state transition matrix which relates state vector perturbations at time, t, to state vector perturbations at time, t_o.

If a navigation measurement is processed at time, t, then $\Delta X(t) = 0$ and $\Delta E(t)$ is computed as a function of the type of measurement, the random errors associated with data processed, and the propagated uncertainty associated with the state vector estimate at the time of a prior measurement or guidance maneuver.

When reasonable confidence is obtained in the trajectory estimate, guidance maneuvers are commanded to restore the dispersed trajectory to specified nominal conditions. If a guidance correction is executed at time, t, $\Delta X(t)$ is computed as a function of the guidance law implemented, the errors associated with the imperfect thrusting maneuver, and the dispersions propagated from the previous navigation measurement or guidance maneuver. $\Delta E(t)$ is calculated as a function of the thrust execution errors and the propagated uncertainties from the previous navigation measurement or guidance maneuver.

If neither a navigation measurement nor a guidance maneuver is commanded, then $\Delta X(t) = \Delta E(t) = 0$, and the error matrices are propagated to the next decision point.

The RMS position and velocity errors, computed from the square root of the trace of either of the aforementioned covariance matrices, are presented in a locally level coordinate system which displays both in-plane and out-of-plane errors. The X-axis of this system is along the radius vector to the spacecraft or probe (radius), the Z-axis is along the orbital angular momentum vector (track), and the Y-axis completes the orthogonal right-handed triad (range). The errors in this system are designated as radius, range, and track errors, and their time rates of change.

RESULTS AND DISCUSSION

Before navigation and guidance analyses can be performed simultaneously for three different missions, navigational measurement types, measurement schedules, and guidance methods which are to be used must be determined. For this study, Earth-based tracking was assumed within the Earth's sphere of influence (ESOI) whereas, outside the ESOI, navigation by an onboard system was assumed. By using onboard navigation outside the ESOI, errors in the ephemerides of the planets could more easily be included. The Earth-injection errors assumed were 4 n. mi. and 16 fps.

The following general discussion refers to the outbound and return midcourse phases of all three missions; discussion of the orbit phase of the 1977 Mars stopover mission is deferred to a later part of the paper. The onboard navigation of the spacecraft was simulated using a sextant for optical angle measurements. During the heliocentric part of the outbound and return trajectories (i.e., the portion between the ESOI and the Mars or Venus sphere of influence, when the Sun is the central body

of the conic), star-planet included angle measurements were processed at 12-hr intervals. Within the sphere of influence of the target planet (Venus or Mars), measurement intervals were reduced to 30 minutes and the type of measurement changed to the star-horizon included angle. These measurement types are discussed in references 4 and 6. The time intervals for the measurement schedules were empirically chosen.

No attempt was made to optimize the choice of stars for the sextant measurements. The star used for each measurement was randomly chosen from a limited catalogue of stars in the simulation program. However, an attempt was made to establish some criteria for the selection of the optimum sighting-body, other than the star, to be used for the optical measurements. This was done by investigating the measurement accuracy obtained by the sextant for bodies of interest along the trajectories of each mission. As pointed out in reference 7, the position uncertainty established with an optical device is directly related to the range of the body being observed. Thus, for each observation the uncertainty in the position measurement for each body of interest can be calculated. By this process, which is based on the range to the observed body and on optical sightings variances, a semi-optimum choice of a sighting body can be made.

Figures are presented which contain the calculated errors in the position measurement for each celestial body of interest during the 1972 Venus flyby, the 1975 Mars flyby, and the 1977 Mars stopover, respectively. By inspection of these plots, a reference navigation schedule of which bodies to sight on can be determined for each mission. The figures presented are applicable only to the three missions in this study; however, a reference navigation schedule can be easily determined in the same manner for any trajectory using similar plots. These figures will be discussed in more detail in the following sections on each respective mission.

After separation of the unmanned probe from the spacecraft during the outbound phase of each mission, navigation of the probe was accomplished by postulating measurements of relative range and range-rate using a radar onboard the spacecraft. For this study the probe entry parameters for each mission were chosen so that the separation ΔV would be a near minimum. However, in actual practice these probe parameters would be chosen as a function of the specific type of mission considered (e.g., hard landing, soft landing, skipout into orbit). For the development of equations pertinent to the probe delivery analysis, refer to appendix A.

1972 Venus Flyby

Spacecraft navigation and guidance.- For outbound and return phases of the Venus flyby mission, the navigation was as previously described for all missions. By inspection of figure 2, a reference schedule was

determined for selecting the sighting body for the star-planet measurements. For example, in figure 2, for the outbound phase of the mission which covers launch to approximately 113 days (Venus periapsis), it is obvious that better measurement accuracy can be obtained by sighting on the Earth from injection until approximately 69 days into the mission, at which time Venus becomes and continues to be the desired sighting body until the return phase. In the return phase, Venus remains the best choice until approximately 210 days into the mission, or about 100 days after Venus periapsis passage, at which time the Earth again becomes the primary sighting body and continues to be until return at Earth. As can be seen, neither the Sun nor Mars aid in decreasing measurement errors.

Typical navigational accuracy data for a Venus mission are contained in figure 3 which shows the spacecraft RMS position uncertainty at Venus periapsis for the outbound phase of the 1972 Venus flyby mission and at Earth periapsis for the return phase. The results of the analysis are presented at only these terminal points of each phase since these are the points of principal interest.

Figure 3(a) contains the projected position uncertainty as a function of the outbound trajectory time. The accuracy degradation caused by the guidance system can be seen by the breaks (denoted by the arrows) in the curve after each guidance maneuver. The initially projected position uncertainty is quite large, as would be expected. However, as can be seen, the error is reduced rather effectively by the Earth-based tracking while the spacecraft is within the ESOI, and remains rather static during the greater part of the heliocentric portion of the trajectory. As has been found from previous studies and the analysis of data for the three missions considered here, the spacecraft position uncertainty tends to decrease slowly with measurements during the heliocentric portion of the trajectory. This tendency seems to be independent of measurement frequency during this period. Conversely, when the spacecraft is within the SOI of the destination planet, the position uncertainty decreases rapidly, varying slightly according to measurement frequency. This is evident in figure 3(a) where one can also see that even with appreciable guidance system degradation during the latter portion of the outbound phase when approaching Venus the onboard navigation system rapidly decreases the uncertainty in spacecraft position estimation at Venus periapsis. It should be noted that the navigation data presented in the conventional manner of total position error at the target represents the combined errors in radius, range, and track. The major portion of the total RMS position errors lies in the down-range component which affects only the arrival time, thus performance, which is mainly a result of altitude error, is generally good even when the total error appears rather large (ref. 2 and 3).

Figure 3(b) contains position uncertainty data for the return phase of the Venus flyby mission similar to that presented for the outbound phase. The RMS position uncertainty at Earth periapsis is presented as a function of time along the return trajectory from Venus periapsis. As can be seen, the position uncertainty curve profile is somewhat different from that

for the outbound phase of the Venus mission. This is partially a result of the longer time of the return phase and of the navigation configuration which utilizes only onboard optical measurements from Venus periapsis passage to the ESOI. The onboard navigation system lowers the initially projected position uncertainty appreciably while within the Venus SOI. However, as can be seen, the error curve tends to level off at a higher value than that for the outbound phase during the heliocentric period of the trajectory. During this time little information is obtainable that will aid the navigation system in decreasing estimation errors. This is evident by looking again at figure 2 in which it can be seen that during the early part of the return phase, the position measurement error of the principal sighting body (Venus) is increasing until approximately 100 days, at which time the Earth becomes the primary sighting body to contribute information which will improve the navigation accuracy. This contribution is shown in the position uncertainty curve of figure 3(b), for at this time a marked decrease is noticed in the curve profile and a continuous decrease in the estimated position error is shown during the remainder of the return phase. Once the spacecraft is within the ESOI, an appreciable increase in estimation accuracy is obtained by the use of the Earth-based tracking. This is evident in figure 3(b), which shows that the RMS position uncertainty for the spacecraft return to Earth is less than 2 n. mi.

Also aiding in the decrease of the final position uncertainty obtained for the return phase was the lack of any significant effect of guidance maneuvers on the navigation system as contrasted to that for the outbound phase. Since this particular mission is continuous, each correction is a reflection of the execution error of the previous correction. Thus, the guidance system degradation to navigational accuracy is decreased with each correction. This is evident by inspection of the curves in figure 3. Notice that the outbound phase shows a significant decrease in position estimation accuracy after each guidance maneuver. However, it is obvious that the effect of the maneuver tends to decrease until, in the return phase, the estimation error curve is only slightly disturbed by a guidance maneuver.

As denoted in figure 3, a total of seven guidance corrections were implemented for the 1972 Venus flyby mission. Only three corrections were needed during the outbound phase to obtain the desired spacecraft delivery accuracy, whereas four corrections were required for the return phase. Figure 4 contains the outbound and return midcourse ΔV as a function of spacecraft delivery accuracy at Venus and Earth, respectively. Each of the figures contains two curves. The solid line represents data obtained in the analysis using VTA guidance within the SOI of the destination planet, whereas the dashed line represents that obtained with the use of FTA guidance. The latter curve is given for comparative purposes only, for in an actual mission FTA guidance would not be used during this particular time period since there is no need to control the down-range error. Also, it is obvious by inspection of figure 4, VTA guidance produces better results for less fuel cost. Thus, discussion will be limited to the curve for VTA guidance. Also, conclusions in this study will be based on the use of VTA guidance during the target planet approach phases.

By inspection of figure 4(a), a total outbound ΔV budget can be determined as a result of the desired periapsis radius dispersion. In this figure the radius of periapsis dispersion at Venus is plotted against total RMS outbound ΔV. The curve representing the VTA guidance plotted in figure 4(a) can be used as an aid in choosing the final correction in the outbound phase. The last point on the curve at the right-hand side of the figure represents the second outbound correction at approximately 8 days from Venus periapsis passage. As can be seen, this second velocity correction resulted in a total ΔV of about 76 fps with a periapsis radius dispersion of 32 n. mi. By following the profile of the dispersion curve, one can easily find whether or not any improvement can be made by a third guidance correction; and, if so, when it should be made. Following the curve from right to left, it is easily seen that in order to reduce the radius of periapsis dispersion to a tolerable value, it is necessary to wait until shortly before Venus periapsis to execute the third velocity correction. In figure 4(a), an arrow denotes the choice of the third correction for this anlysis. That is, for a ΔV of approximately 11 fps executed at 4 hours from periapsis, a delivery accuracy of 4 n. mi. can be acquired at Venus periapsis, resulting in a total midcourse fuel cost of 96 fps for the outbound phase of the mission. The choice denoted is considered to be the best since the dispersion gets no better and the required ΔV increases rapidly after this point. This lower bound of the delivery accuracy is very dependent on the accuracy of the navigation system.

Figure 4(b) consists of information for the return phase of the 1972 Venus flyby plotted in the same manner as for the outbound phase. Thus, the total return ΔV and the placement of the fourth, or final guidance correction for the return phase can be determined in a similar manner. In this figure, the radius of periapsis dispersion at Earth is plotted as a function of the total RMS return ΔV. Again, it is advantageous to wait until a few hours from periapsis to initiate the final velocity correction. By inspection of the curve representing VTA guidance, it is evident that the best delivery accuracy that can be obtained is approximately 1 n. mi. This accuracy would, in turn, cost only 30 fps more than had been expended after the third correction; or it would cost a total of 116 fps for the return phase of the 1972 Venus flyby mission. The time choice for the fourth correction is again denoted in figure 4(b) by an arrow. The improvement of the dispersion at Earth in the return phase as compared to that at Venus during the outbound phase is a result of the improved navigation accuracy from longer onboard tracking during the heliocentric period and from Earth-based tracking with the ESOI.

The figures previously discussed for the 1972 Venus flyby indicate that spacecraft delivery accuracies of 4 n. mi. and 1 n. mi. can be obtained at Venus periapsis in the outbound phase and at Earth periapsis in the return phase, respectively. These accuracies represent corridors of 24 and 6 n. mi. at the respective targets. The cost of obtaining these

delivery accuracies was approximately 96 fps for the outbound phase and 116 fps for the return phase resulting in a total cost of 212 fps for midcourse maneuvers in the 1972 Venus flyby mission.

Unmanned probe navigation and guidance.- A plot of pertinent probe entry parameters as a function of separation velocity is presented for the 1972 Venus flyby mission in figure 5. It was assumed that the probe would be deployed from the spacecraft at the Venus SOI (≈330 000 n. mi. from the planet) and that the inclination of the probe trajectory would be the same as that of the spacecraft flyby hyperbola. The minimum separation velocity occurs when the angle between $\Delta\bar{V}_{SEP}$ and the spacecraft velocity vector is 90°. Figure 5(a) presents probe entry data for an entry altitude of 490 000 ft; an entry altitude of 580 000 ft is assumed for the data presented in figure 5(b). The increase in the entry altitude has the effect of shifting all curves to the left so that the minimum separation velocity occurs for a smaller entry speed for the increased entry altitude. Variations in the entry flight-path angle from 0° to -45°, for fixed entry speed and altitude, produce an increase in the required separation velocity and a decrease in the time required for the probe to "arrive" at vacuum periapsis.

The choice of the probe entry trajectory has a definite effect on the delivery accuracy but a parametric study to determine this influence was beyond the scope of this note. For the analysis presented the probe entry parameters were chosen such that a near-minimum separation velocity would be required. The entry altitude, speed, and flight-path angle specified were 490 000 ft, 37 670 fps, and -10°, respectively, with a corresponding separation ΔV of 50 fps. With this choice of entry parameters the probe would arrive at its vacuum periapsis approximately 3 minutes after the spacecraft reaches the periapsis of the flyby hyperbola.

The probe navigation results for this mission are presented in figure 6. The significance of plotting the vacuum periapsis radius error is better understood if one realizes that this single parameter is a measure of the entry corridor attainable by the probe midcourse navigation or guidance system (entry corridor = vacuum periapsis radius error multiplied by factor of six). The uncertainty and dispersion in this parameter are performance indices for the probe navigation and guidance systems respectively. The effect of the onboard radar accuracy on the vacuum periapsis radius uncertainty is illustrated in this figure. The difference between the nominal radar errors (σ_ρ = 50 ft, $\sigma_{\dot{\rho}}$ = 0.5 fps,) and the 2× nominal errors (σ_ρ = 100 ft, $\sigma_{\dot{\rho}}$ = 1.0 fps) is most pronounced around 14 hours from separation. The two curves converge, however, after 28 hours of tracking (56 measurements).

The probe midcourse guidance results are illustrated in figure 7. Only the data for the nominal radar tracking errors are presented since the

midcourse ΔV profile for the 2× nominal radar errors is essentially the same as the data shown. A single correction executed 1.5 hours before the probe would arrive at its vacuum periapsis requires a ΔV of 35 fps with a resulting corridor of 22.2 n. mi. (vacuum periapsis radius dispersion = 3.7 n. mi.). If this correction is delayed 1 hour, the corridor attainable by the midcourse guidance system can be reduced to 19.8 n. mi. for an increased ΔV cost of 108 fps.

1975 Mars Flyby

Spacecraft navigation and guidance.- The 1975 Mars flyby mission is similar to the Venus flyby mission. The outbound phase is 133 days, and the return phase is 539 days, resulting in a total round-trip time of 672 days. The navigation and guidance assumed for the 1975 Mars flyby was that previously discussed for all missions. Similarly, the optimum sighting body schedule for the star-planet measurements was chosen by inspection of a plot of measurement accuracies obtained by the sextant for bodies of interest along the trajectory. Figure 8 was used to determine this reference schedule for the 1975 Mars flyby mission. It is easily seen in this figure that the Earth is the planet to use for the first 80 days of the outbound phase of the mission. At this time Mars becomes the prominent body and continues to be until almost 500 days into the mission, or about 360 days into the return phase. From this point, Earth again is the obvious choice. As can be seen, these two bodies (i.e., Earth and Mars) do not at all times contribute significant information to the navigation system; however, no other body along the trajectory at any time does even as well as these two. The effects of the fluctuations in the measurement error curves of figure 8 can be seen in the following navigation accuracy curves.

Figure 9 contains typical navigation data for a Mars flyby mission. Figures 9(a) and 9(b) contain the spacecraft RMS position uncertainty at Mars periapsis for the outbound phase and at Earth periapsis for the return phase of the 1975 Mars flyby, respectively. As for the Venus mission, the results here are presented only at terminal points of each phase.

As can be seen in figure 9(a), the obtained navigation accuracy for the outbound phase of the Mars flyby is very similar to that shown for the Venus flyby. The initially projected error is very large, but is reduced effectively early in the mission. The effects of the guidance system degradation can also be seen after each guidance maneuver (denoted by arrows). Unlike the Venus outbound phase, the Mars flyby outbound phase requires a total of four velocity corrections to obtain the specified corridor at Mars periapsis. In figure 9(a), one can see that the final RMS position uncertainty is approximately 40 n. mi. This uncertainty is

twice the value obtained for the previous mission and is partially a result of the spacecraft's shorter trajectory time within the Mars SOI. However, as previously mentioned, the largest portion of the error in position is in the down-range component which results in an arrival timing error; thus it does not affect the performance of the spacecraft.

Navigation data for the return phase of the 1975 Mars flyby is presented in figure 9(b). These data are plotted in the same manner as in figure 9(a). Although the return phase is several hundred days longer than the outbound phase, four velocity corrections are sufficient. The uncertainty curve profile behaves in much the same manner as that for the return phase of the Venus mission. Again the guidance system degradation is much less during the return phase and again the total RMS position uncertainty is reduced to approximately 1 n. mi. at Earth periapsis.

A total of eight guidance maneuvers was required for the round trip of the 1975 Mars flyby. Four corrections were needed for each phase to obtain the desired spacecraft delivery accuracy at each respective planet. Figure 10(a) and (b) contains the outbound and return midcourse ΔV as a function of spacecraft delivery accuracy at Mars and Earth, respectively. As for the Venus mission, solid line curves represent data obtained with VTA guidance, and dashed line curves represent that obtained with FTA guidance. For this Mars flyby mission, only the VTA guidance data will be discussed.

By inspection of figure 10, a total outbound and return ΔV budget can be determined as a result of the desired periapsis radius dispersion at the respective targets. In figure 10(a), the radius of periapsis dispersion at Mars is plotted against total RMS outbound ΔV. Since the data plotted here begins after the third outbound velocity correction, the VTA guidance data curve can be used for choosing the final correction of the outbound phase. After the third correction, represented by the last point on the right-hand side of the plot, the total outbound RMS ΔV used was 60 fps, and a delivery accuracy of approximately 37 n. mi. can be obtained. However, since the third correction was executed 24 hours before Mars periapsis passage and since the value of total ΔV used thus far is still rather low, it is obvious that a fourth velocity correction can be executed such that a safe delivery accuracy can be obtained. Thus, using the same criteria as was used in the Venus mission, possibly the best choice for the fourth guidance maneuver is at 5 hours from periapsis passage. By inspection of figure 10(a), it can be seen that for approximately 12.5 fps more, or a total outbound RMS ΔV of 82.5 fps, a radius of periapsis dispersion of less than 4 n. mi. can be obtained.

Similarly, from figure 10(b) the final velocity correction in the return phase of the 1975 Mars flyby can be chosen. The total return ΔV is dependent on the choice of corrections made and the accuracy obtained during the outbound phase since the flyby is a continuous mission.

Figure 10(b) consists of information for the return phase of the 1975 Mars flyby. In this figure, the radius of periapsis dispersion at Earth is plotted against total RMS return ΔV. Having already executed three velocity corrections during the return phase at a cost of 136 fps for a delivery accuracy of 50 n. mi., one can choose the final correction time from the VTA guidance data curve in figure 10(b). As can be seen, the best accuracy that can be obtained is approximately 1 n. mi. For this delivery accuracy a fourth correction must be made almost 3.5 hours from Earth periapsis at a cost of 35 fps, resulting in a total RMS return ΔV of 171 fps. As pointed out in the discussion of the Venus mission, the delivery accuracy is very dependent on the navigation system accuracy; thus the use of Earth-based tracking during the approach-to-Earth upon returning significantly aids in the improvement of the delivery accuracy as compared to that at Mars in the outbound phase.

The figures presented for the 1975 Mars flyby mission indicate that a manned spacecraft can be delivered to specified targets at Mars and Earth within accuracies of 4 n. mi. and 1 n. mi., respectively. For this mission, the costs represented by these accuracies were approximately 83 fps for the outbound phase and 171 fps for the return phase, resulting in a total cost of 254 fps for midcourse maneuvers.

Unmanned probe navigation and guidance.- A plot of pertinent probe entry parameters as a function of separation velocity is presented for the 1975 Mars flyby mission in figure 11. The probe was assumed to be deployed from the spacecraft at the Mars SOI ($\approx$312 000 n. mi. from the planet) with the probe trajectory inclination the same as the inclination of the spacecraft flyby hyperbola. Figure 11(a) presents probe entry data for an entry altitude of 315 000 ft; an entry altitude of 405 000 ft is assumed for the data presented in figure 11(b).

The probe reference trajectory characteristics for the navigation and guidance analysis presented were an entry altitude, speed, and flight-path angle of 315 000 ft, 32 250 fps, and $-10°$; the separation ΔV was 14 fps. With this choice of entry parameters the probe would arrive at vacuum periapsis 2 minutes before the spacecraft reaches the periapsis of the flyby hyperbola.

The probe navigation results for nominal and 2× nominal onboard radar errors are presented in figure 12. The 2× nominal radar errors degrade the projected estimate of the vacuum periapsis radius during most of the tracking period and the two curves eventually converge to the same value 18 hours after separation (36 measurements).

The midcourse guidance results for this mission are presented in figure 13. Figure 13(a) presents the guidance data for the nominal radar errors, and 13(b) illustrates the guidance data for 2× nominal onboard radar errors. A single correction executed 48 minutes before the probe

would reach vacuum periapsis produces a target dispersion of 4.1 n. mi. for a ΔV cost of 81 fps (σ_ρ = 50 ft, $\sigma_{\dot{\rho}}$ = 0.5 fps); increasing the radar errors by a factor of two and computing the effect of a single correction at this same time produces a resulting radius dispersion of 6.8 n. mi. at vacuum periapsis for the same ΔV. This indicates that, for this mission, an increase in radar tracking errors could have a pronounced effect on the guidance corridor. For example, if the specified guidance corridor is 30 n. mi. then the increase in tracking errors could result in the probe not hitting the specified conditions. This corridor could be attained, however, in the case of the increased tracking errors, if the correction is delayed for 30 minutes. Then the corridor could be reduced to 19.8 n. mi. (radius dispersion = 3.3 n. mi.) with an increased ΔV penalty of 195 fps.

1977 Mars Stopover

Spacecraft navigation and guidance.- This stopover mission consists of a 360-day outbound phase, a 300-day stopover orbit phase, and a 320-day return phase. The orbital phase will be discussed separately; whereas, the outbound and return phases are discussed together, as for the two other missions, for ready comparison.

The navigation and guidance system configuration assumed for the outbound and return phases of the 1977 Mars stopover mission was that previously discussed for all missions. Using the plotted position measurement error in figures 14(a) and (b), a reference schedule of the optimum sighting body for the star-planet measurements was chosen for the outbound and return phases, respectively. Figure 14(a) contains the error in position measurement as a function of time from injection at Earth. It can be seen that the Earth is the optimum body for the onboard optical measurements during the first 140 days of the outbound trip phase. From this time until Mars periapsis, the planet Mars is the optimum body. Similarly in figure 14(b), it is evident that for the return phase the optimum sighting body choice is Mars for the first 220 days and Earth for the remaining trip time.

Navigational uncertainty data for the 1977 Mars stopover outbound and return phases can be found in figures 15(a) and 15(b), respectively. These figures are similar to those containing the same type data for the Venus and Mars flyby missions. The principal difference can be seen in the slightly higher initial and intermediate uncertainty values for both the outbound and return phases. This, of course, is a direct result of the much longer time periods of both phases of the 1977 Mars stopover as compared to those for the previous missions. Also, it should be remembered that there is a time period of 300 days between the end of the outbound phase and the beginning of the return phase.

Figures 15(a) and 15(b) contain the RMS position uncertainty at Mars periapsis and at Earth periapsis as functions of time along the outbound and return trajectories, respectively. Each phase required four guidance maneuvers to meet the specified delivery accuracy requirements. (These velocity corrections are denoted by arrows.) As can be seen in these figures the terminal position uncertainty for each phase is approximately equal to that of each respective phase of the two previous missions. In figure 15(b), again notice the leveling-off of the curve profile during the long heliocentric period of the return phase when very little navigation information is obtained, and the appreciable drop in the curve at approximately 220 days when the Earth again becomes the optimum sighting body.

Figures 16(a) and 16(b) contain the total outbound and return RMS ΔV as a function of RMS radius of periapsis dispersion at Mars and Earth, respectively. These figures were used to determine the fourth correction of each phase of the 1977 Mars stopover mission in the same manner as was done for the Venus and Mars flyby missions. That is, in figure 16(a) it can be seen that after the third velocity correction of the outbound phase, the delivery accuracy of the spacecraft to Mars periapsis (or orbit deboost) is 26 n. mi., and the total cost at this time is 74 fps. By following the VTA guidance data curve to the left of the figure, it is evident that a delivery accuracy of approximately 4 n. mi. can be obtained by a fourth guidance maneuver executed at 3.5 hours from orbit deboost for the added cost of only 20 fps or a total outbound fuel cost of 90 fps.

Similarly, using figure 16(b), for the return phase a delivery accuracy of less than 1 n. mi. can be obtained by making a fourth guidance correction at 2.5 hours before Earth periapsis for a total return cost of approximately 80 fps.

It should be noticed that in comparing the outbound and return phases of the three missions the terminal delivery accuracies of all three missions are approximately equal; however, the cost of midcourse guidance maneuvers is considerably less in the 1977 Mars stopover mission than in the two previous missions. This is a result of the basic characteristics of the 1977 Mars stopover mission, especially the time length, low speed, and trajectory configuration. Table II presents a comparison of the characteristics of these missions.

Spacecraft navigation and guidance (orbit phase).- As was previously mentioned the 1977 Mars stopover mission includes a 300-day stay time in orbit about the planet Mars. The characteristics of this orbit are presented in table III.

Since a navigation and guidance analysis for the Mars orbital phase warrants a complete study within itself, only a brief sketch of orbital navigational data and no guidance data are presented.

There are several types of orbital navigation techiniques which are applicable to this study (see ref. 8); however, for the data presented only one type of navigation was considered for the spacecraft while in orbit about Mars. The navigation simulated was the star-Mars-horizon included angle measured with a sextant. These measurements were processed throughout the 300-day stay time at 1-hour intervals. This particular measurement should be quite applicable to the particular mission being studied since the apoapsis of the orbit is approximately 10 000 n. mi. from Mars and the orbital period is about 0.5 day.

The navigational data obtained for the 300-day orbital phase of the 1977 Mars stopover is presented in figure 17, in which the RMS position uncertainty is plotted as a function of time in orbit. By inspection of figure 17, it is found that the star-horizon navigation measurement controls the RMS position uncertainty to a range between approximately 0.6 and 3.0 n. mi. (1σ). The interesting feature of the figure is the oscillatory behavior of the uncertainty curve. No specific reason is given for this effect, although it is probably geometrical with respect to the planet's orbit as well as that of the spacecraft. The oscillation directly resulting from each orbit is not shown in the figure because of the scale.

Unmanned probe navigation and guidance.- A plot of pertinent probe entry parameters as a function of separation velocity is presented for the 1977 Mars stopover mission in figure 18. Figure 18 presents the entry data for entry altitudes of 315 000 ft and 405 000 ft.

The nominal probe trajectory selected for this mission assumed an entry altitude of 315 000 ft, an entry speed of 18 350 fps, and an entry flight-path angle of $-5°$. The probe deployment ΔV was 45 fps.

The unmanned probe navigation results are presented in figure 19, for both nominal and 2× nominal onboard radar errors. The 2× nominal radar errors produce lower projected vacuum periapsis radius uncertainties between 35 and 50 hours from separation. The explanation for this phenomena is related to the correlation in the augmented uncertainty matrix for the spacecraft-probe combination. The behavior of the data is as expected outside of this time period, and the two curves converge to the same value approximately 58 hours from separation (116 measurements).

The guidance results for nominal and 2× nominal radar errors are illustrated in figures 20(a) and 20(b), respectively. The increased radar tracking errors have the effect of doubling the ΔV cost to achieve a specified target dispersion. For example if a corridor of 30 n. mi. is desired (vacuum periapsis radius dispersion = 5 n. mi.), the ΔV cost for nominal radar errors is 25 fps whereas for 2× nominal radar errors the cost is increased to almost 50 fps.

CONCLUDING REMARKS

Navigation and guidance analyses for three representative manned interplanetary missions - a 1972 Venus flyby, a 1975 Mars flyby, and a 1977 Mars stopover - were presented. All phases of each mission were considered; an evaluation of the performance of both the manned spacecraft and an unmanned probe was included for each mission.

The purpose of the study was not to recommend any specific mission, but rather to show several different interplanetary missions and the similar navigation and guidance results obtained.

Excluding the fuel cost for maneuver in the Mars stopover orbit phase, the results indicate for each mission that a total midcourse ΔV of the order of 200 fps (1σ) can produce spacecraft delivery accuracies of approximately 4 n. mi. at Mars or Venus and 1 n. mi. at Earth for the outbound and return mission phases, respectively. Similarly, an accuracy somewhat less than 5 n. mi. is indicated for a probe delivery with one midcourse correction costing approximately 80 fps (1σ).

TABLE I.- NOMINAL RMS ERROR VALUES (1σ)

(a) Navigation system

Onboard sextant accuracy, arc sec	10
Onboard radar accuracy:	
Range, ft	50
Range rate, fps	0.5
Radius uncertainty/planet radius:	
Mars, Venus	0.005
Earth	0.001
Planet position uncertainty, n. mi.	100
Earth-based radar accuracy:	
Range, ft	$20 \leq$ range ≤ 200
Range rate, fps	$0.5 \leq$ range rate ≤ 1.5

(b) Guidance system

Proportional, percent	1
Pointing, deg	1
Cutoff, fps	0.5

TABLE II.- REFERENCE TRAJECTORY CHARACTERISTICS

Trajectory designation	1972 Venus flyby	1975 Mars flyby	1977 Mars stopover
Julian date of launch from Earth	2 441 410.0	2 442 675.0	2 443 400.0
Earth injection velocity magnitude, fps	12 131	15 150	12 652
Outbound trip time, days	111.03	133.29	360
Target planet stopover time, days	0	0	300
Return trip time, days	251.64	538.64	320
Time in target planet sphere of influence, hr	60.73	37.74	(+300 days in orbit) 199.4
Periapsis altitude at target planet, n. mi.	206	106	200
General location of periapsis at target planet (with respect to target planet equator)		Northern Hemisphere	Southern Hemisphere
Entry velocity at Earth, fps	44 840	47 900	38 463

TABLE III.- CHARACTERISTICS OF STOPOVER ORBIT
OF 1977 MARS MISSION

Orbit staytime, days	300
Periapsis altitude, n. mi.	200
Apoapsis altitude, n. mi.	9621.67
Inclination, deg	18.65
Eccentricity, n.d.	.697
Period, hr	11.78
Periapsis velocity in (hyperbola), fps	17 800
Periapsis velocity (ellipse), fps	14 403
Apoapsis velocity (ellipse), fps	2568
Periapsis velocity out (hyperbola), fps	18 395

TABLE IV.- MIDCOURSE ΔV AND TARGET PLANET DISPERSION SUMMARY

Mission	Phase	RMS midcourse ΔV, fps					RMS target planet dispersions, n. mi.		
		ΔV_1	ΔV_2	ΔV_3	ΔV_4	Total	Radius	Range	Track
1977 Mars stopover	Outbound	45.95	16.13	12.04	[a]14.42	88.54	3.89	448.00	1.45
	Return	22.35	12.51	21.43	[a]21.03	77.32	0.68	1030.04	0.23
1975 Mars flyby	Outbound	43.14	10.26	6.10	[a]22.55	82.05	3.88	81.73	3.83
	Return	32.26	24.45	78.64	[a]36.30	171.75	1.09	871.04	0.71
1972 Venus flyby	Outbound	50.44	25.95	[a]19.77	--	96.16	4.09	121.16	1.47
	Return	35.36	20.54	29.81	[a]30.97	116.68	0.99	389.68	0.59

[a]These corrections used VTA guidance.

TABLE V.- PROBE ΔV AND DISPERSION SUMMARY

Mission	Onboard radar error	Separation ΔV, fps	Midcourse ΔV, fps	Total ΔV, fps	Vacuum periapsis radius dispersion, n. mi.
1977 Mars stopover	Range = 50 ft Range-rate = 0.5 fps	45.57	62.65	108.22	3.06
	Range = 100 ft Range-rate = 1.0 fps	45.57	61.13	106.70	4.34
1975 Mars flyby	Range = 50 ft Range-rate = 0.5 fps	14.32	81.11	95.43	4.13
	Range = 100 ft Range-rate = 1.0 fps	14.32	80.90	95.22	6.87
1972 Venus flyby	Range = 50 ft Range-rate = 0.5 fps	49.39	51.87	101.26	3.51
	Range = 100 ft Range-rate = 1.0 fps	49.39	51.58	100.97	3.60

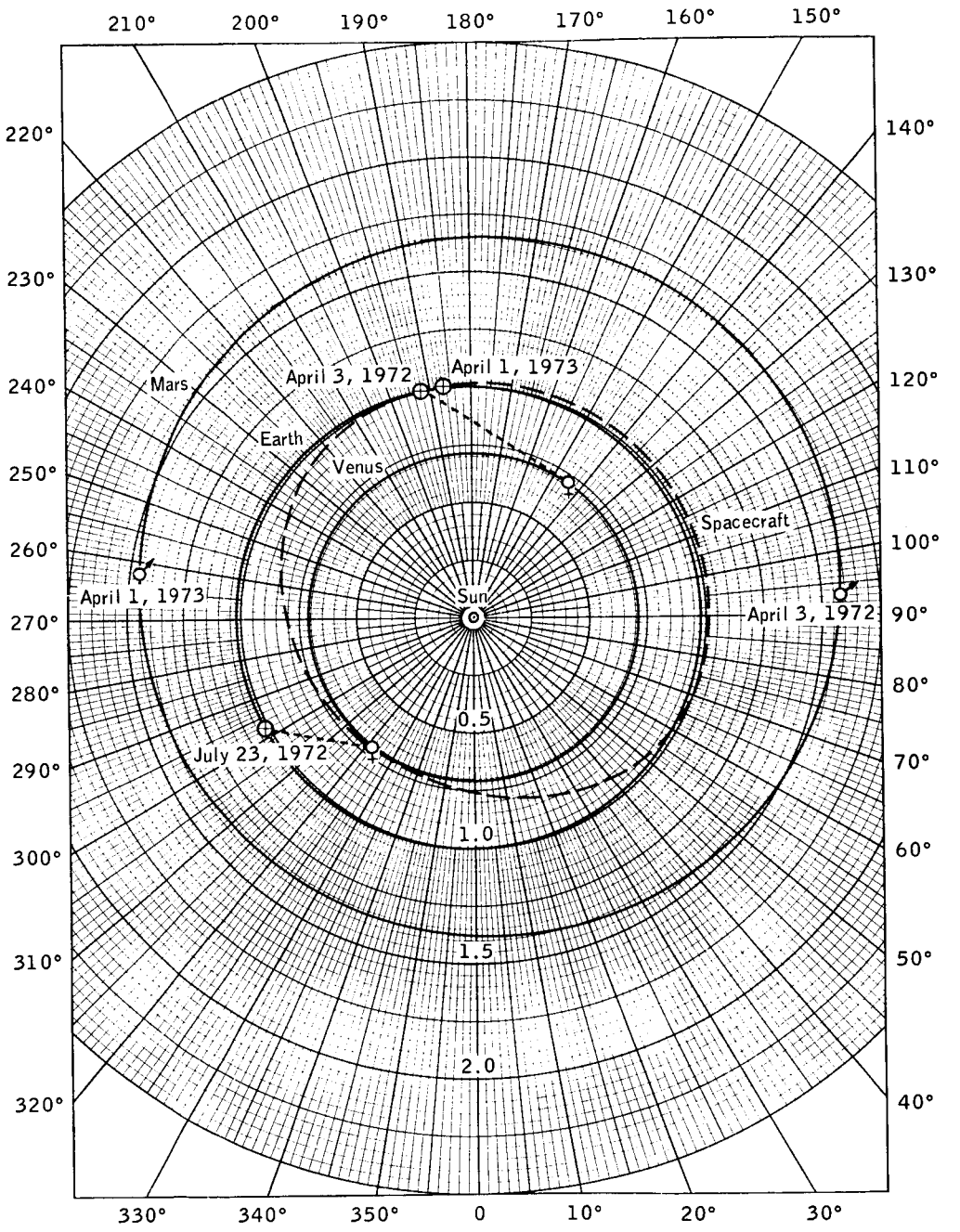

(a) 1972 Venus flyby.

Figure 1. - Projection of trajectories into the ecliptic plane.

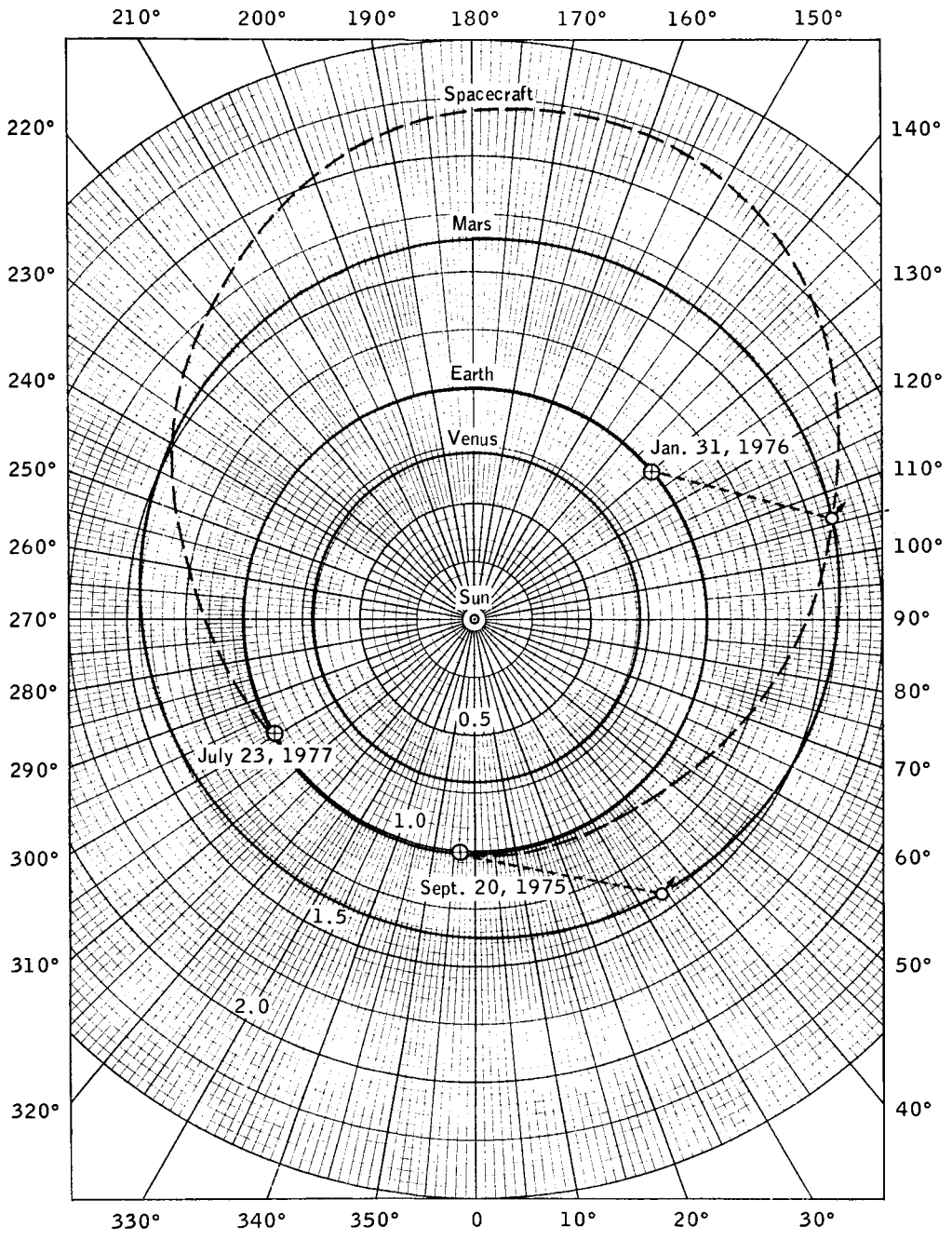

(b) 1975 Mars flyby.

Figure 1. - Continued.

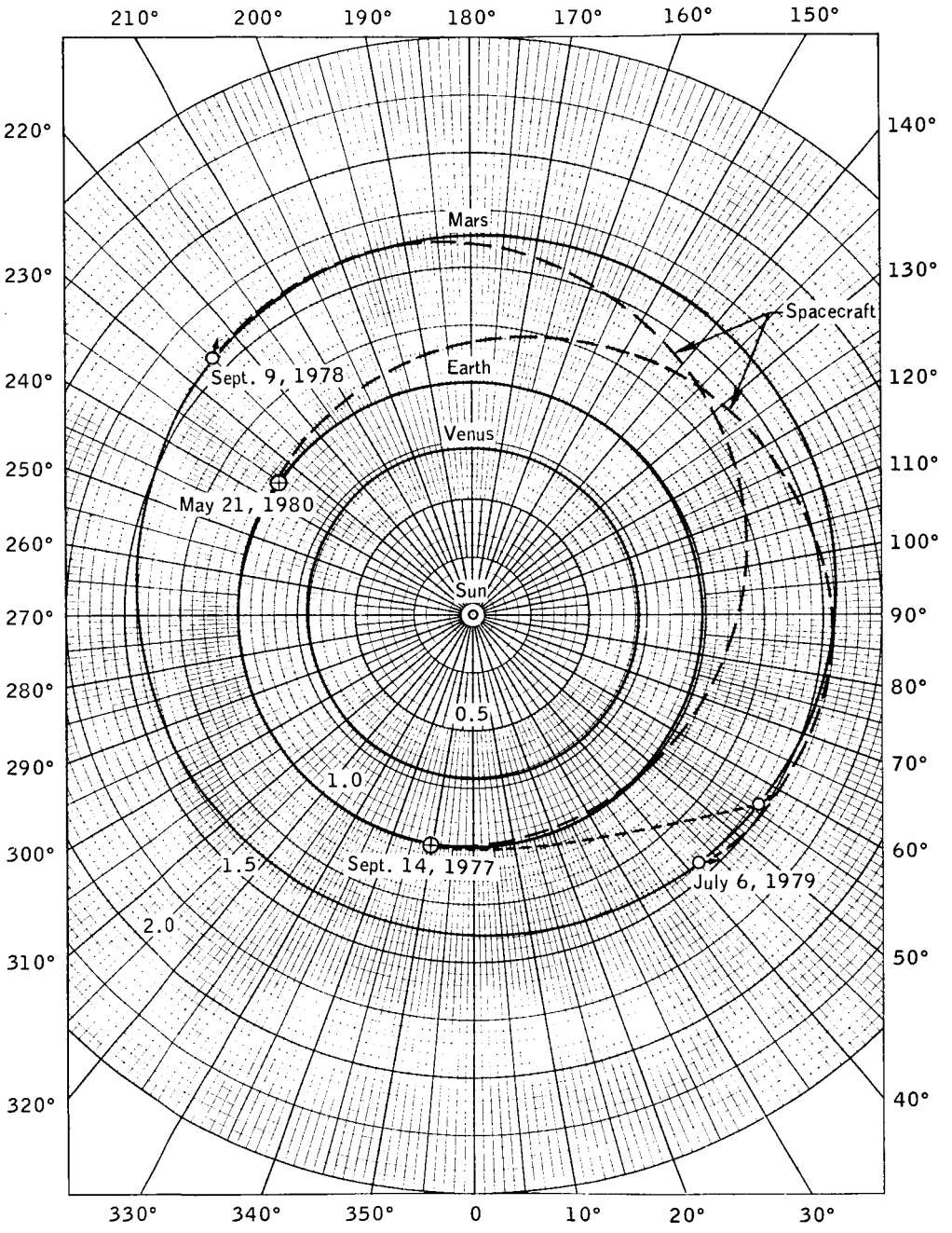

(c) 1977 Mars stopover.

Figure 1. - Concluded.

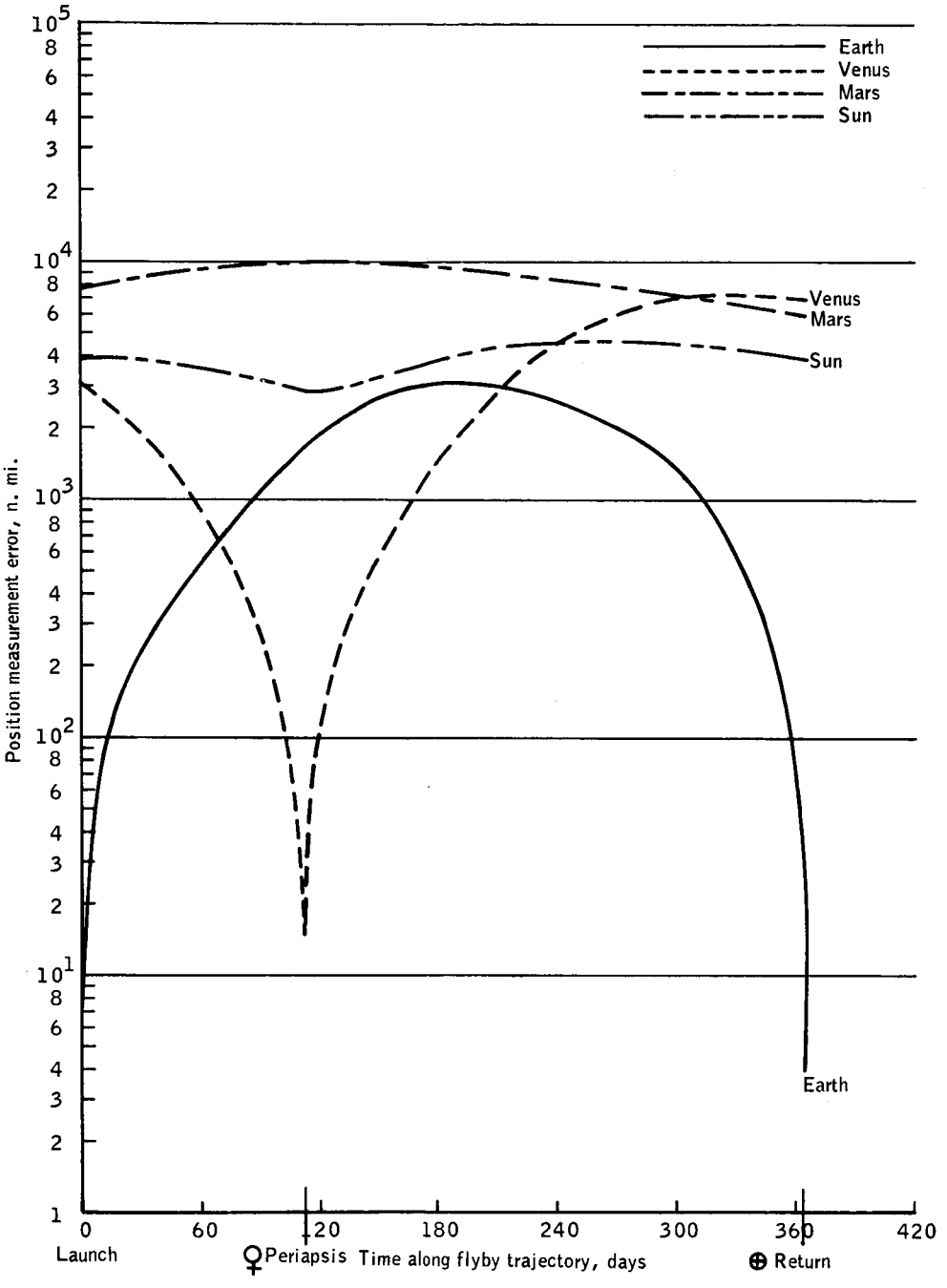

Figure 2.- Sighting-body position measurement errors used to determine navigation schedule for 1972 Venus flyby trajectory.

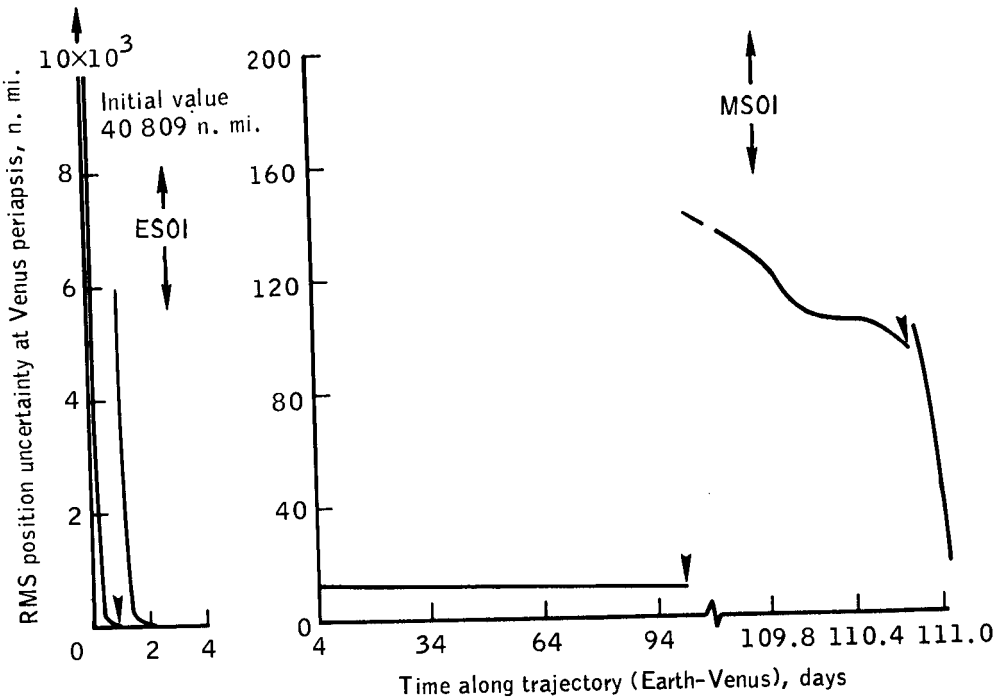

(a) Earth-Venus trajectory (outbound).

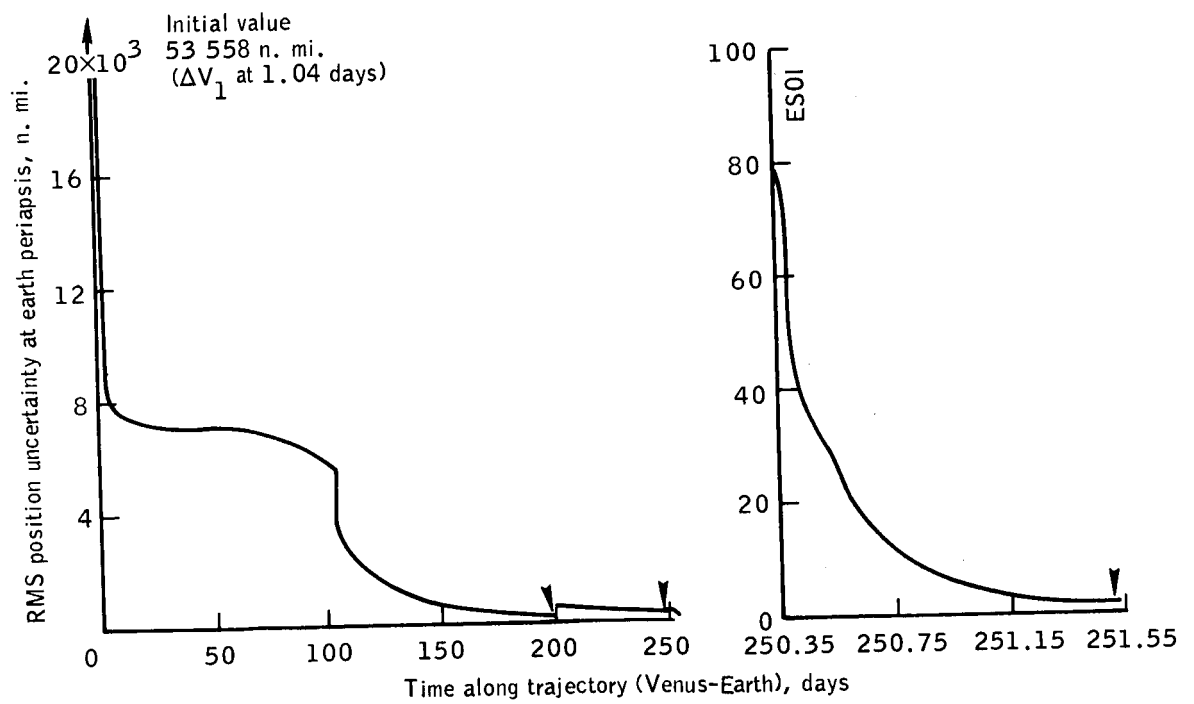

(b) Venus-Earth trajectory (return).

Figure 3.- RMS position uncertainty at target planet periapsis for 1972 Venus flyby.

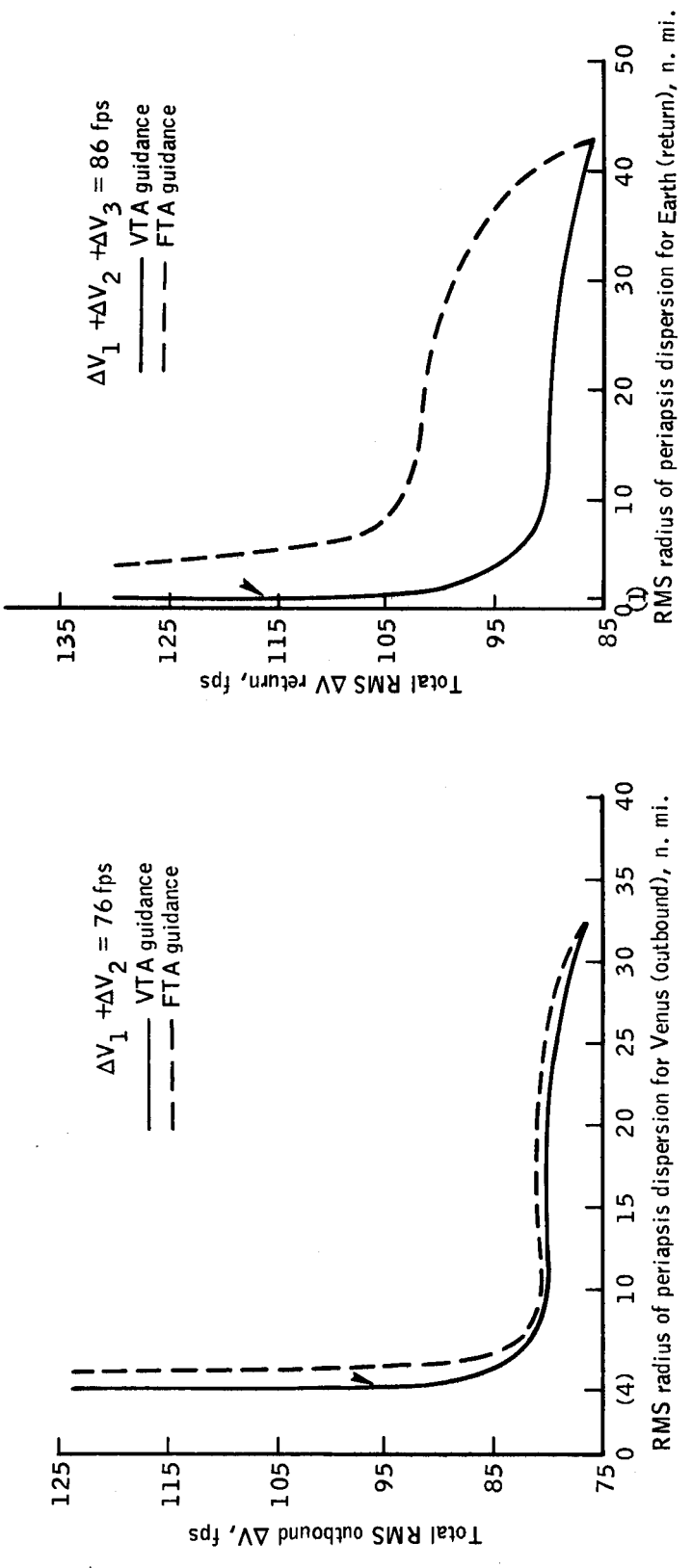

(a) Venus approach phase (outbound).

(b) Earth approach phase (return).

Figure 4.- Spacecraft guidance accuracy for 1972 Venus flyby.

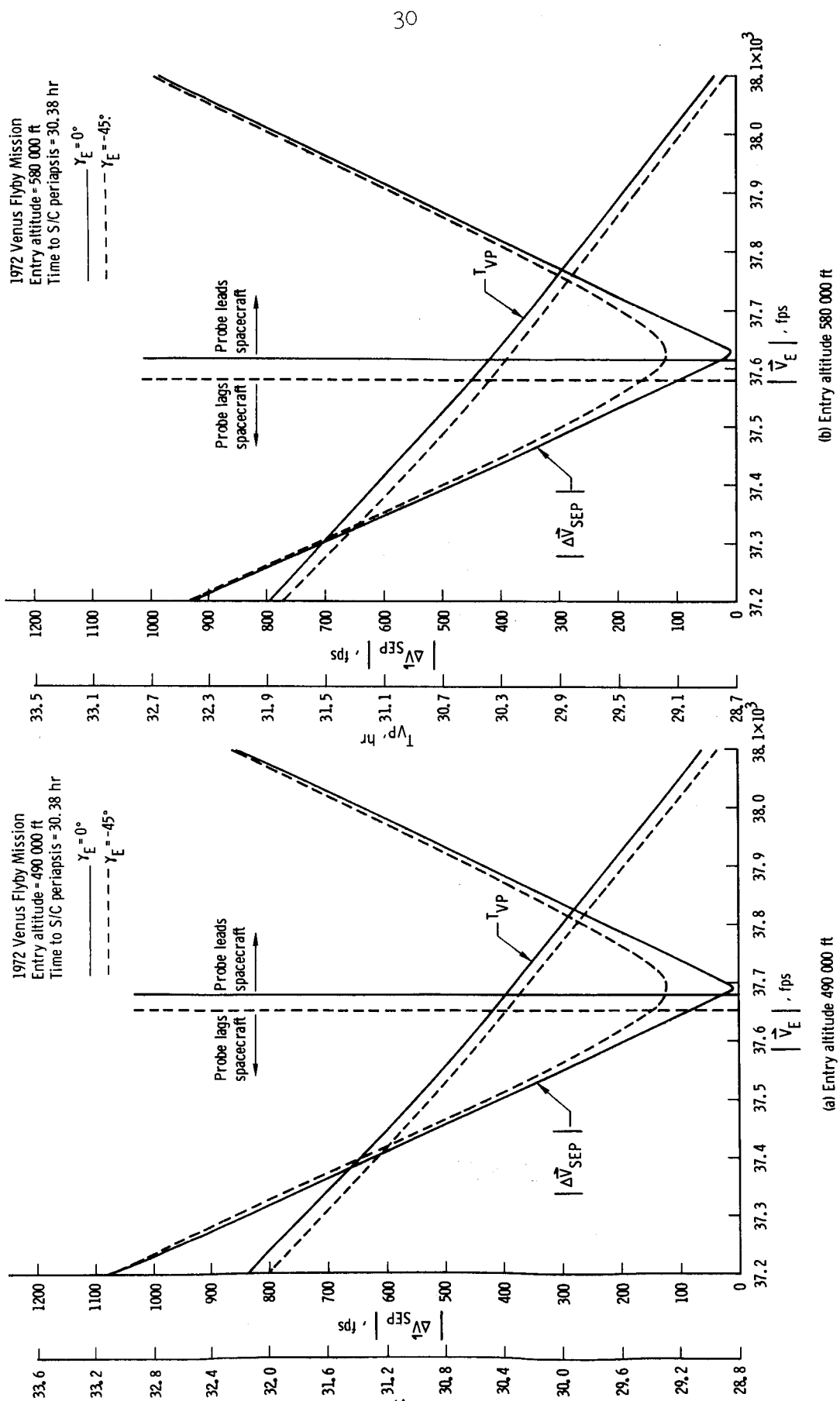

(a) Entry altitude 490 000 ft

(b) Entry altitude 580 000 ft

Figure 5. - Unmanned probe entry parameters as a function of separation velocity for 1972 Venus flyby.

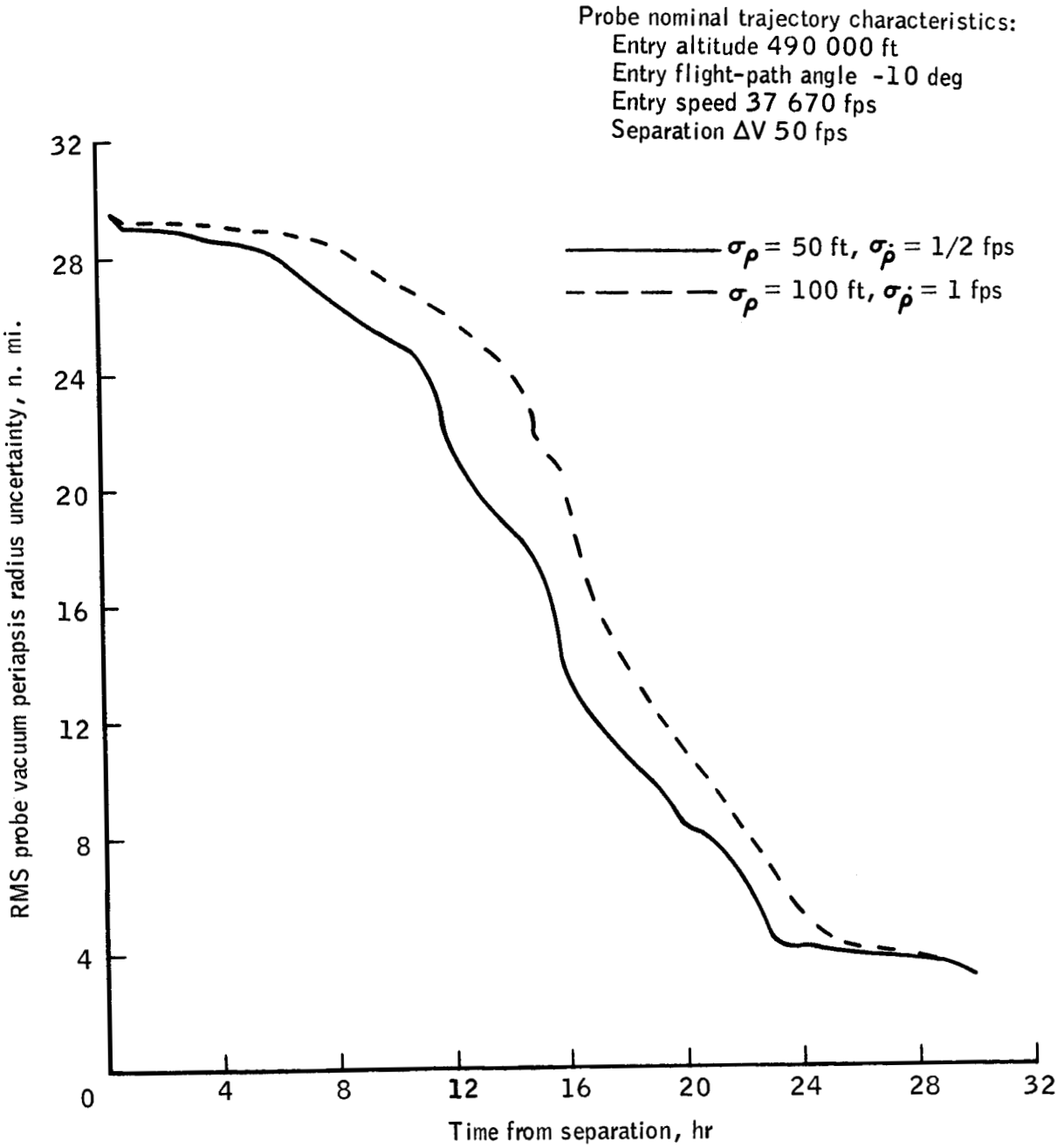

Figure 6.- Probe navigation data for 1972 Venus flyby.

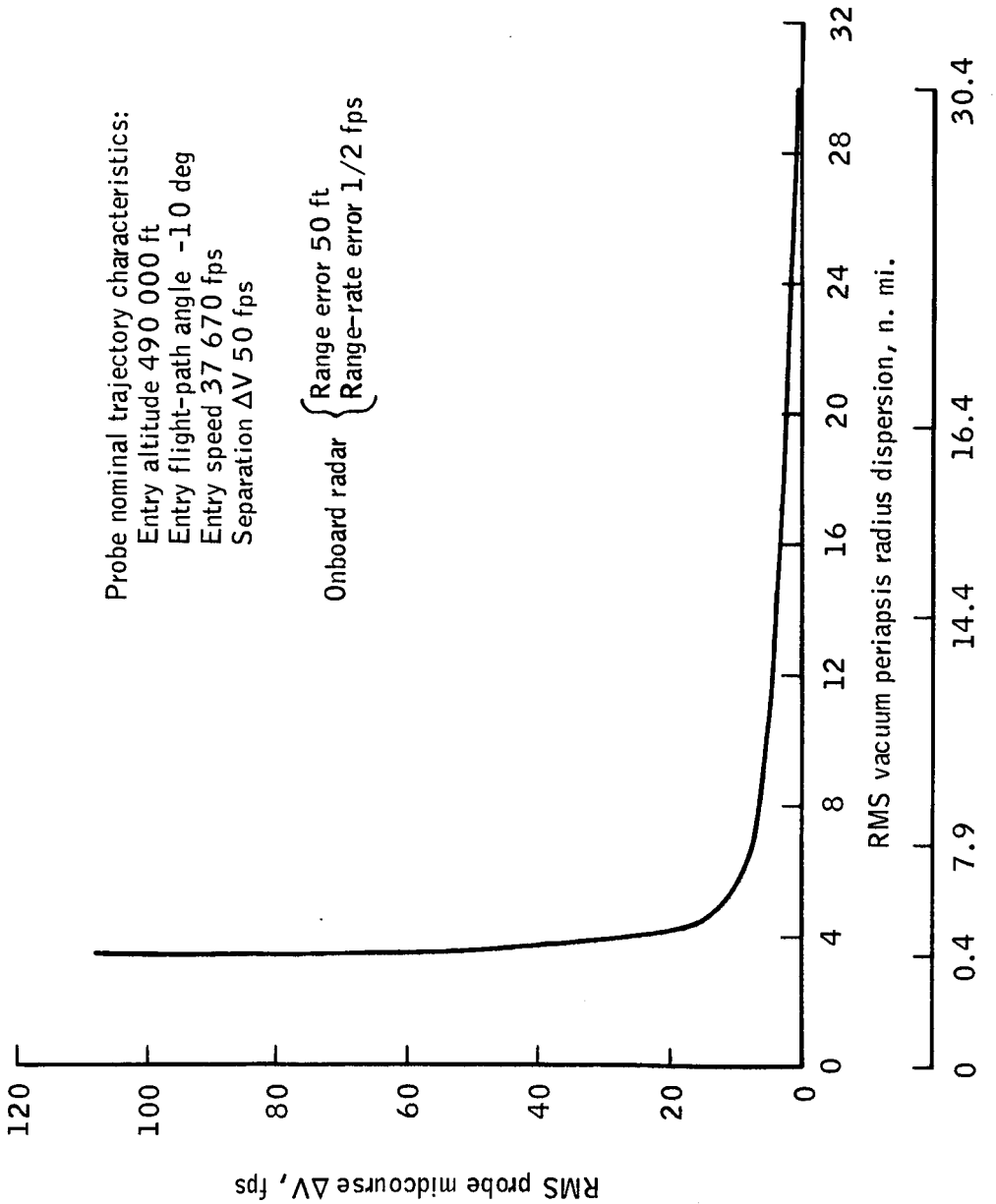

Figure 7.- Probe guidance data for 1972 Venus flyby.

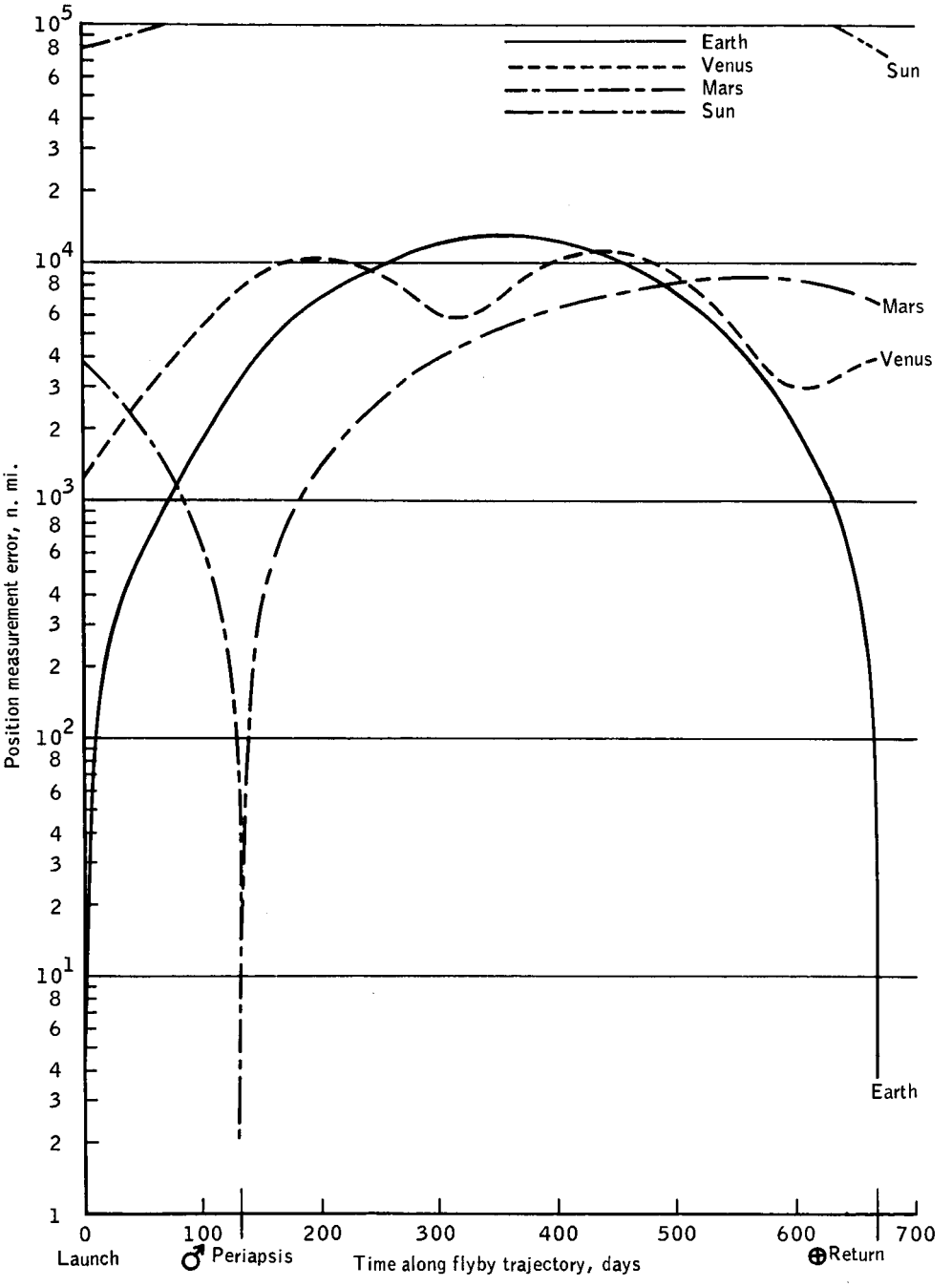

Figure 8.- Sighting-body position measurement errors used to determine navigation schedule for 1975 Mars flyby trajectory.

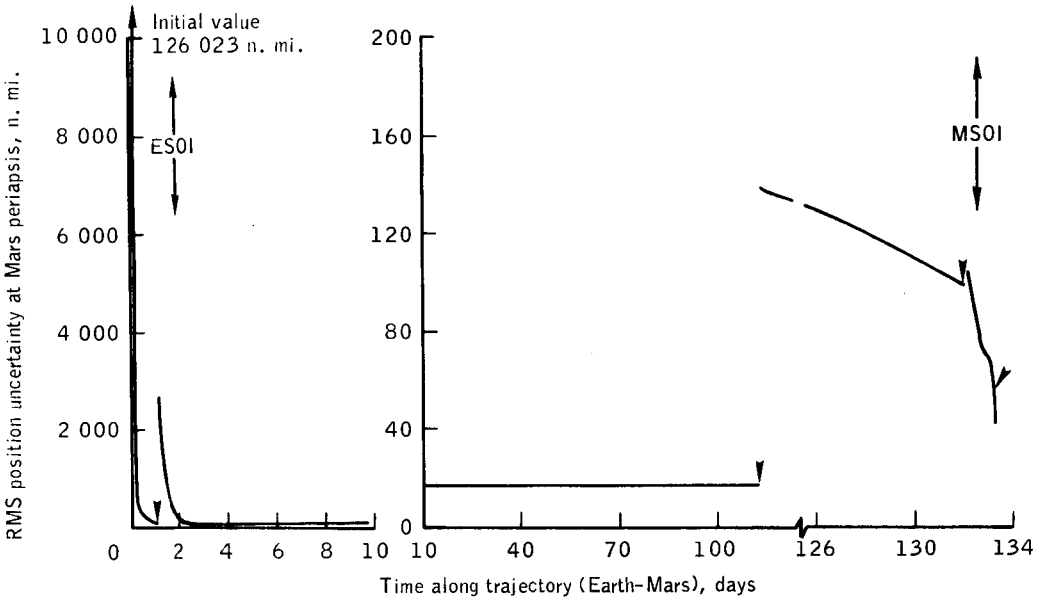

(a) Earth-Mars trajectory (outbound).

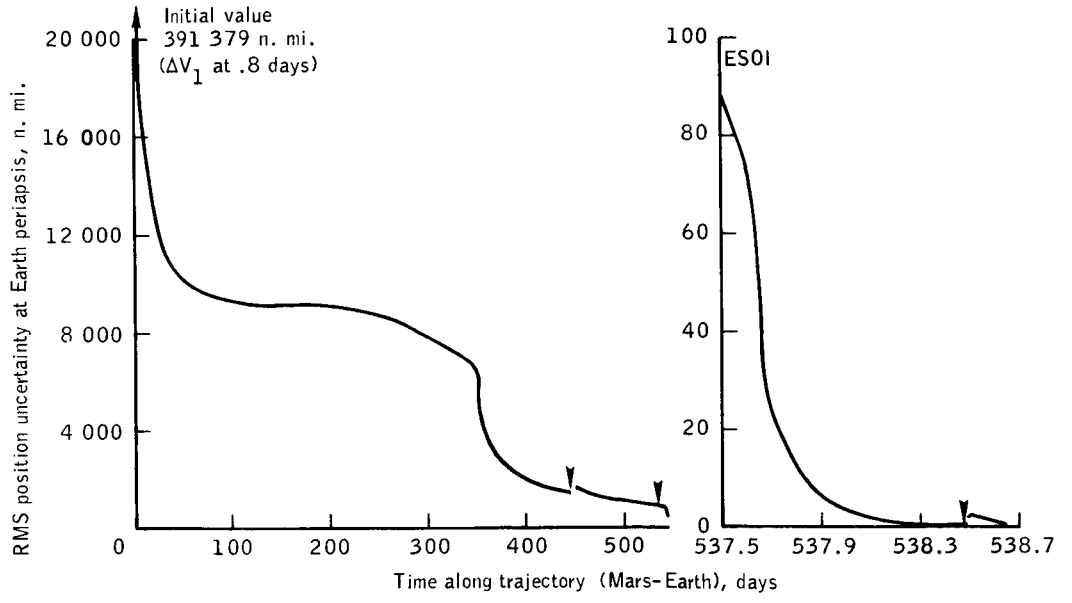

(b) Mars-Earth trajectory (return).

Figure 9.- RMS position uncertainty at target planet periapsis for 1975 Mars flyby.

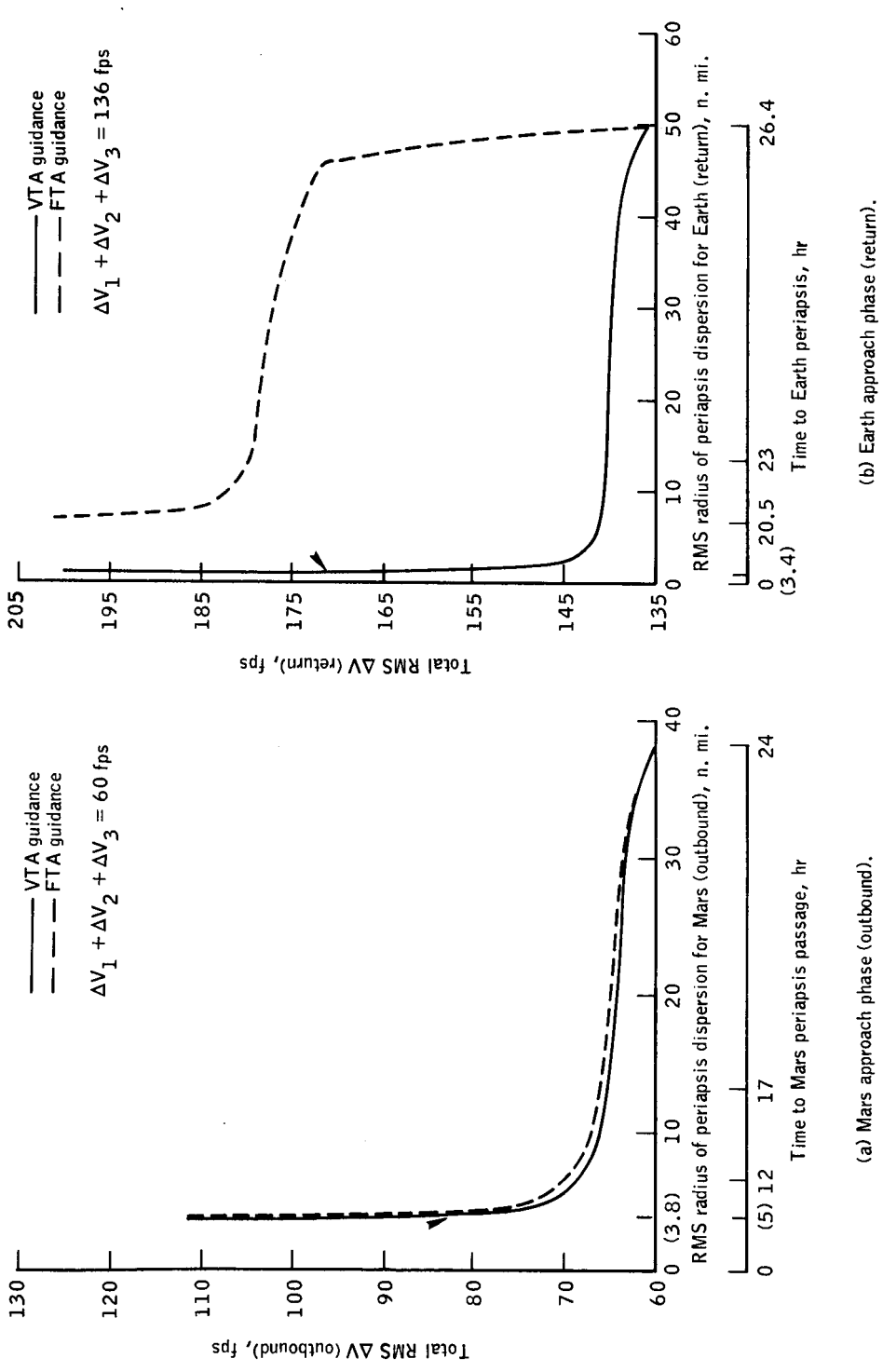

(a) Mars approach phase (outbound).

(b) Earth approach phase (return).

Figure 10.- Spacecraft guidance accuracy for 1975 Mars flyby.

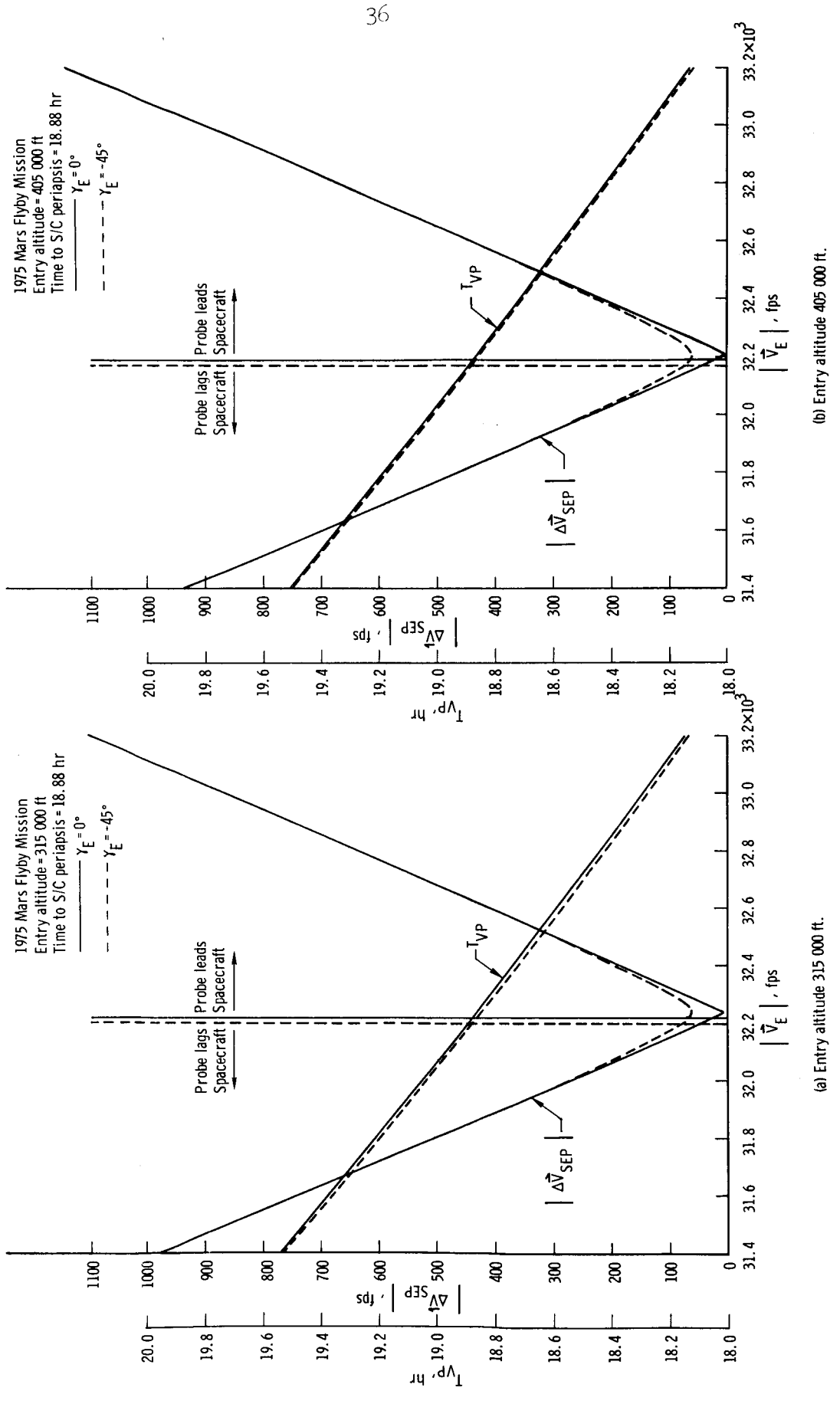

(a) Entry altitude 315 000 ft.

(b) Entry altitude 405 000 ft.

Figure 11. - Unmanned probe entry parameters as a function of separation velocity for 1975 Mars flyby.

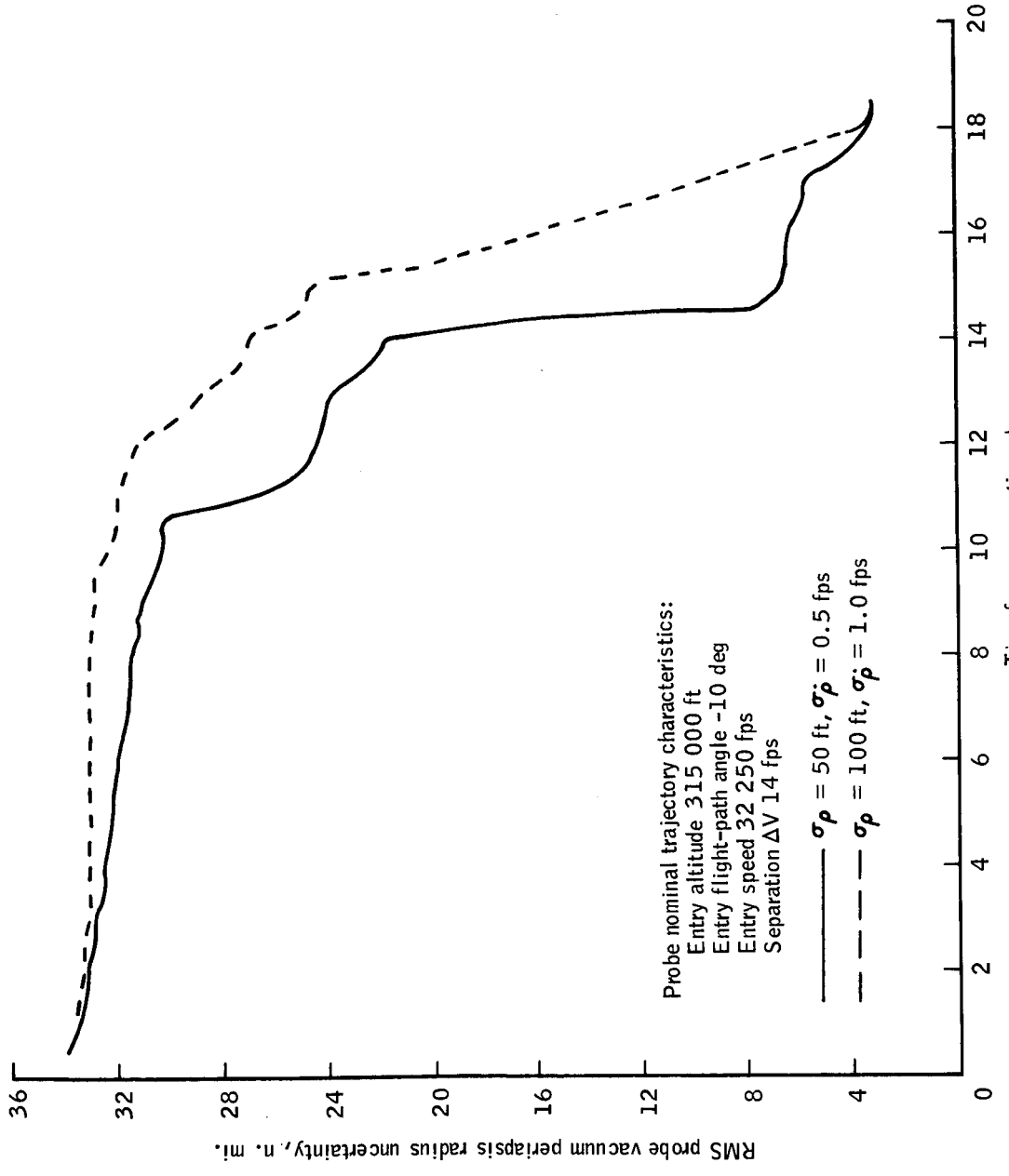

Figure 12.- Probe navigation data for 1975 Mars flyby.

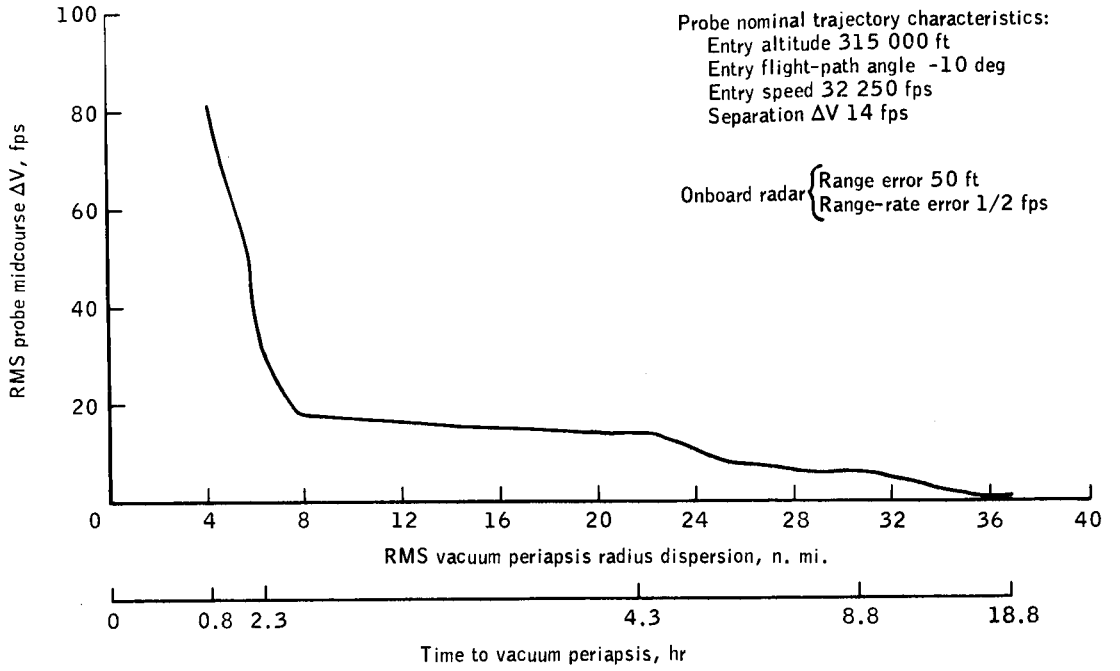

(a) Nominal onboard radar errors.

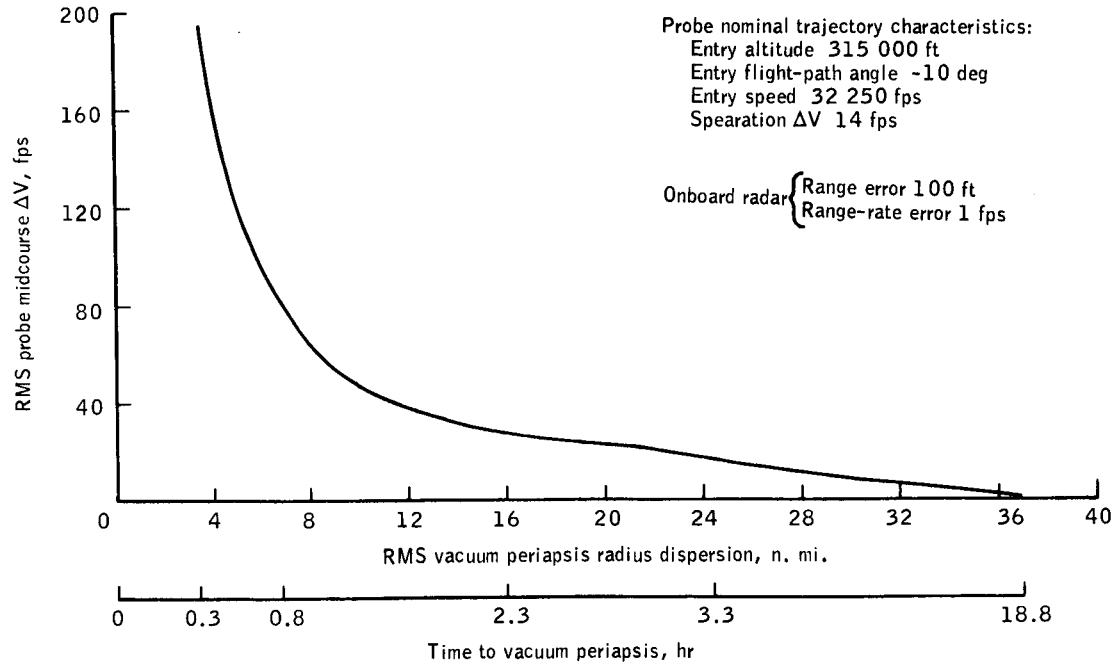

(b) 2X nominal onboard radar errors.

Figure 13.- Probe guidance data for 1975 Mars flyby.

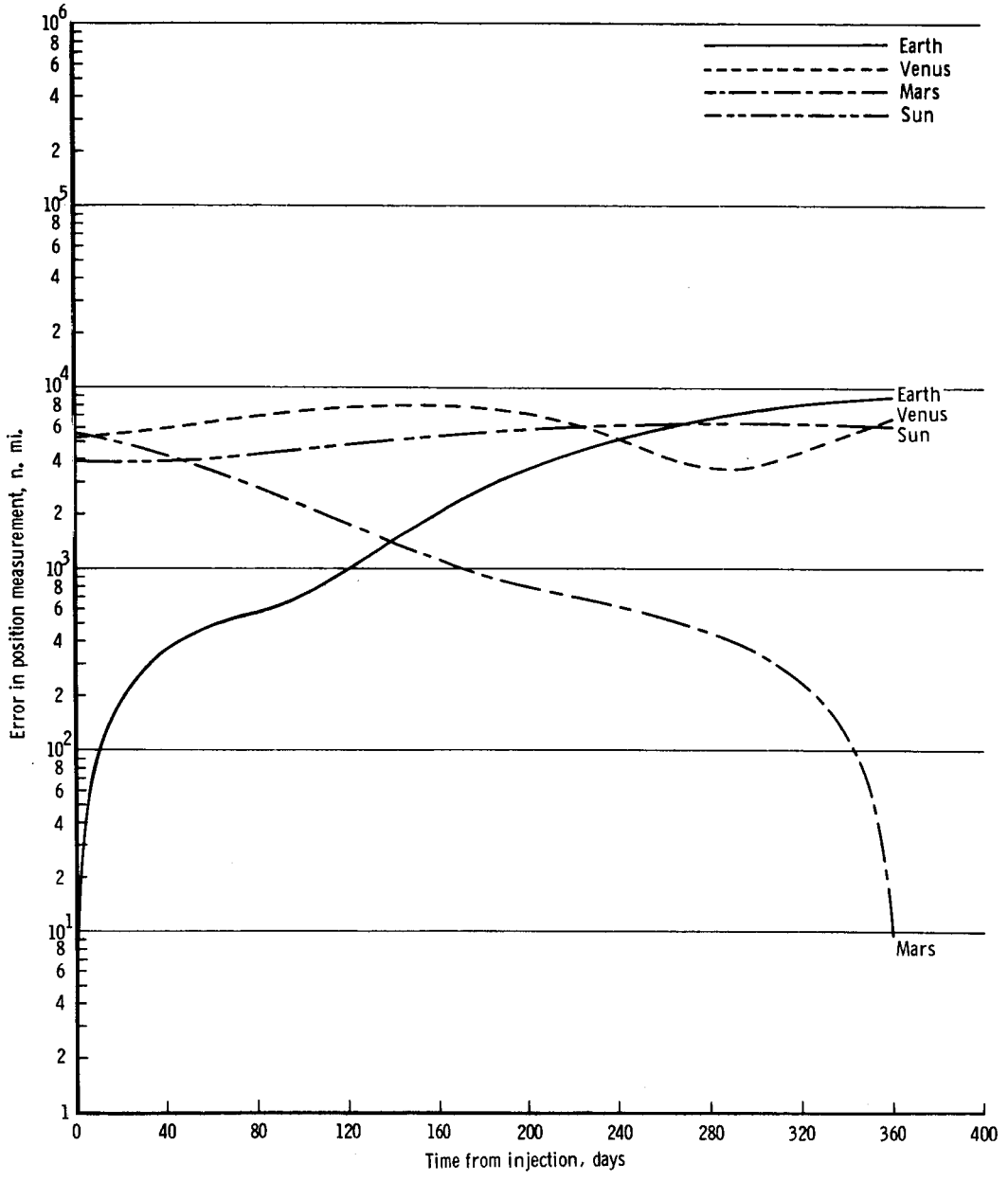

(a) Earth-Mars trajectory (outbound).

Figure 14. - Sighting-body position measurement errors used to determine navigation schedule for 1977 Mars stopover trajectory.

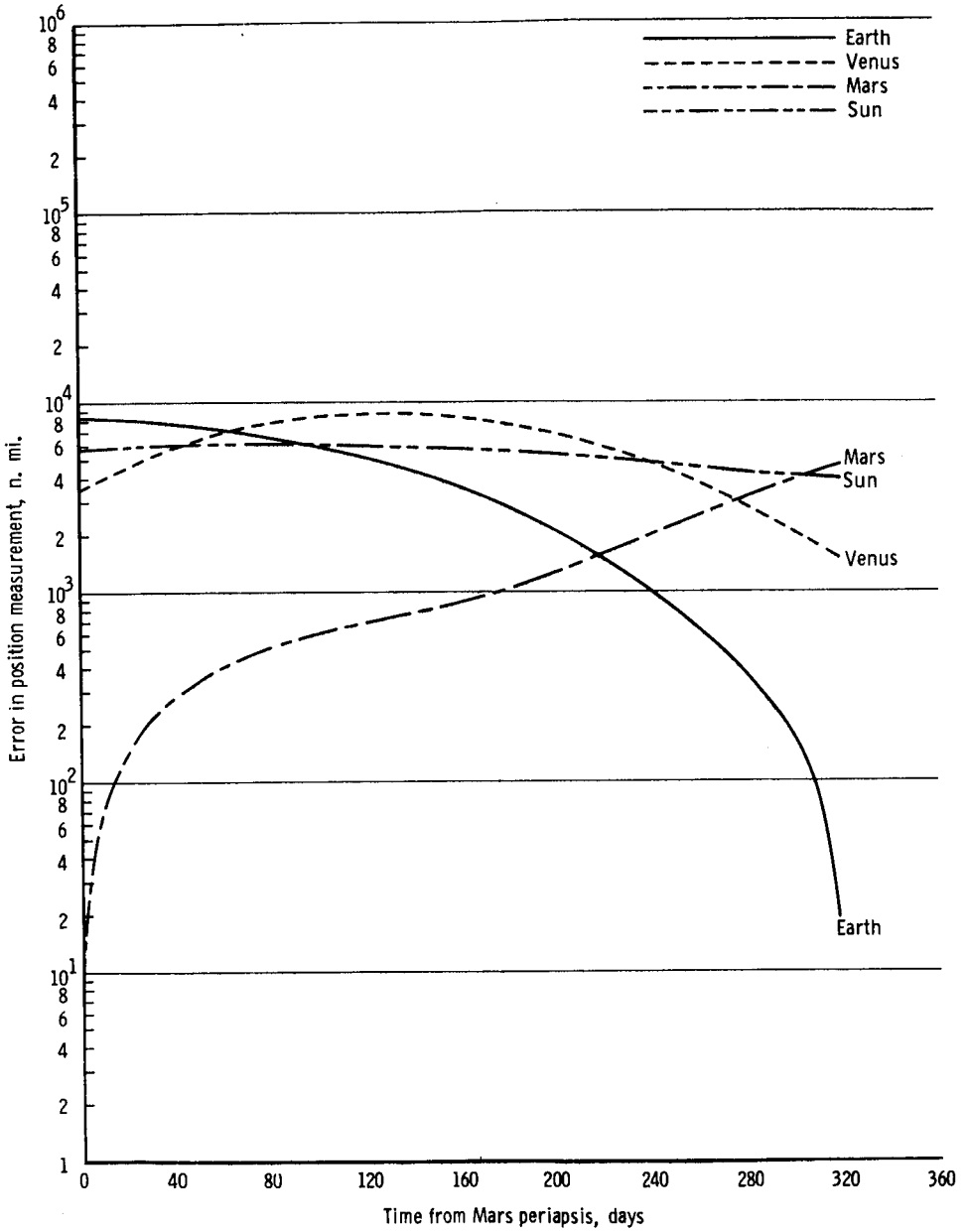

(b) Mars-Earth trajectory (return).

Figure 14. - Concluded.

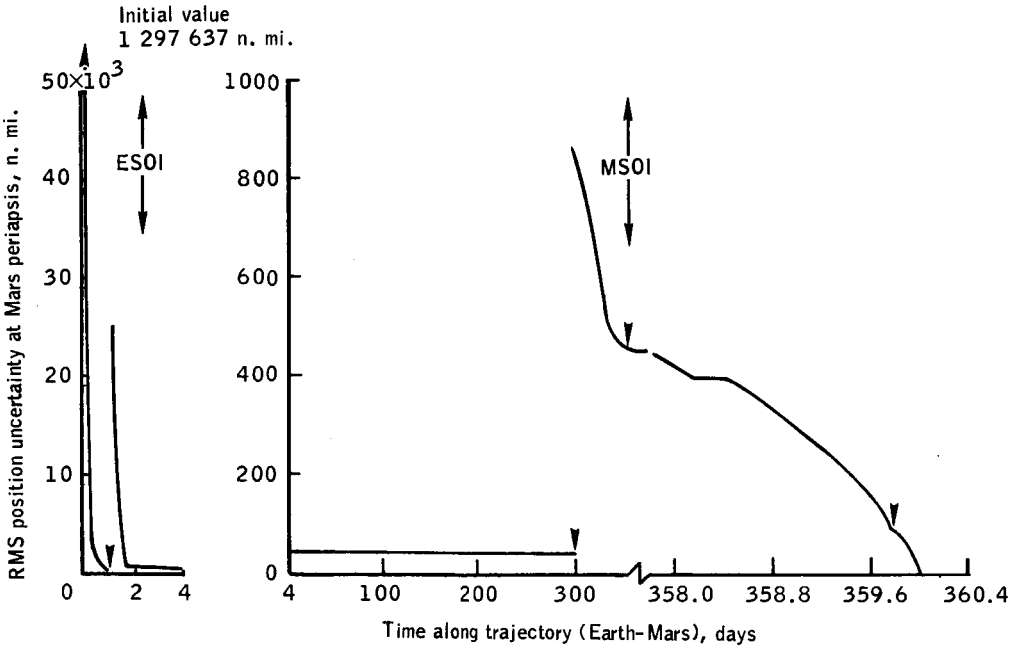

(a) Earth-Mars (outbound)

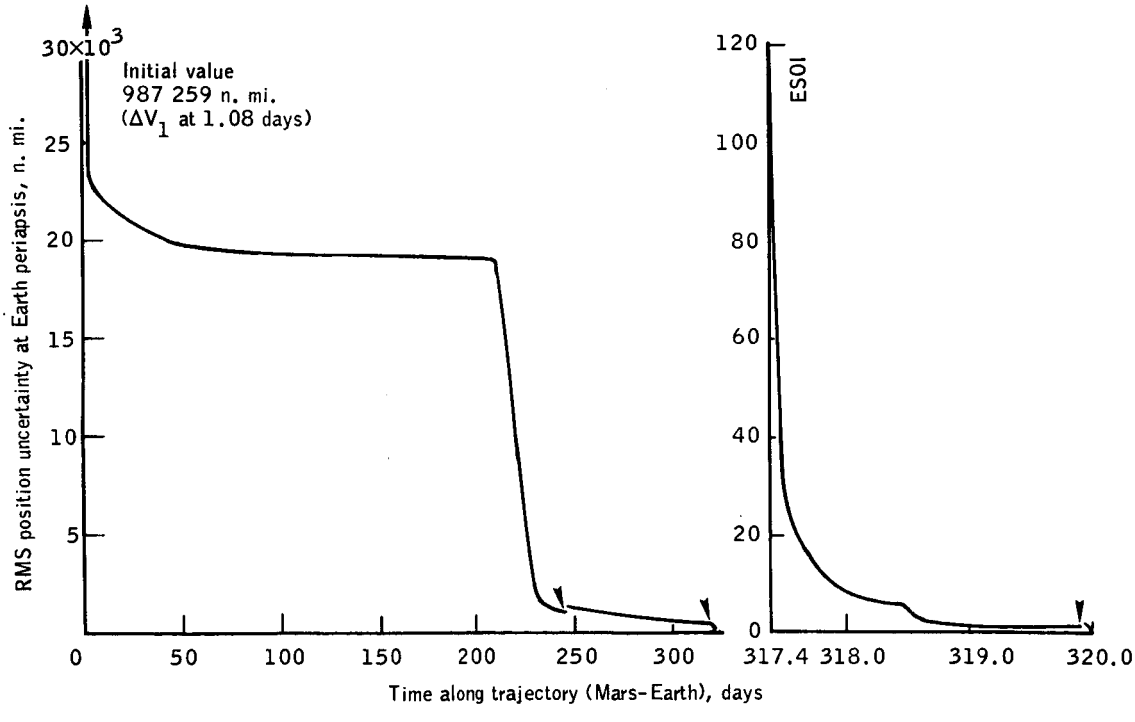

(b) Mars-Earth (return)

Figure 15.- RMS postion uncertainty at target planet periapsis for 1977 Mars stopover.

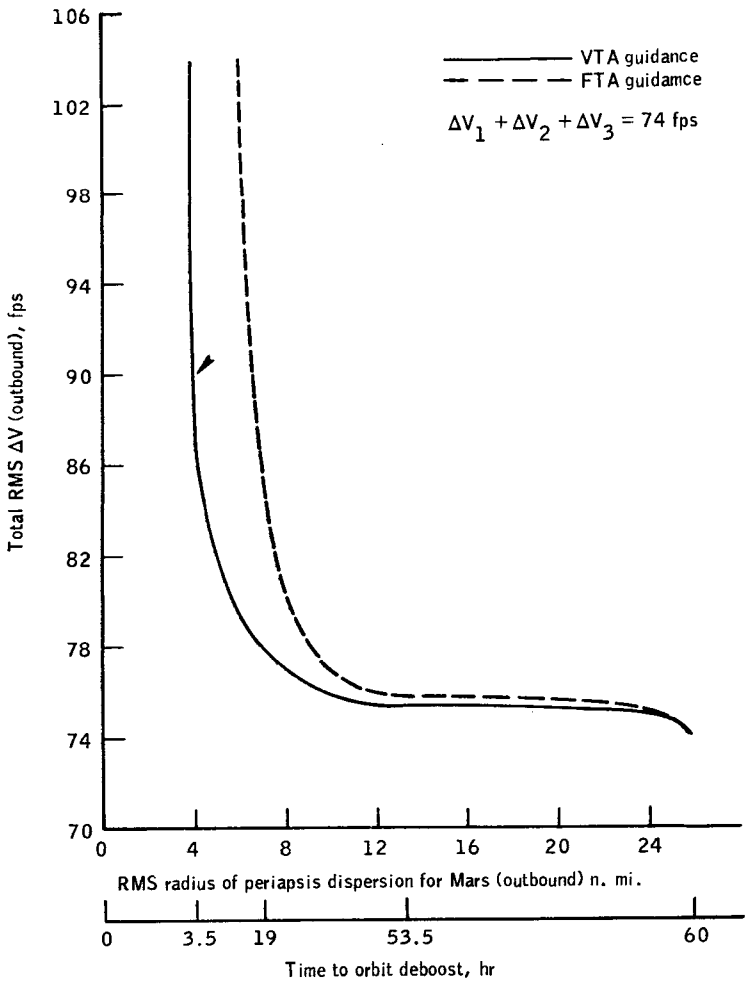

(a) Mars approach phase (outbound).

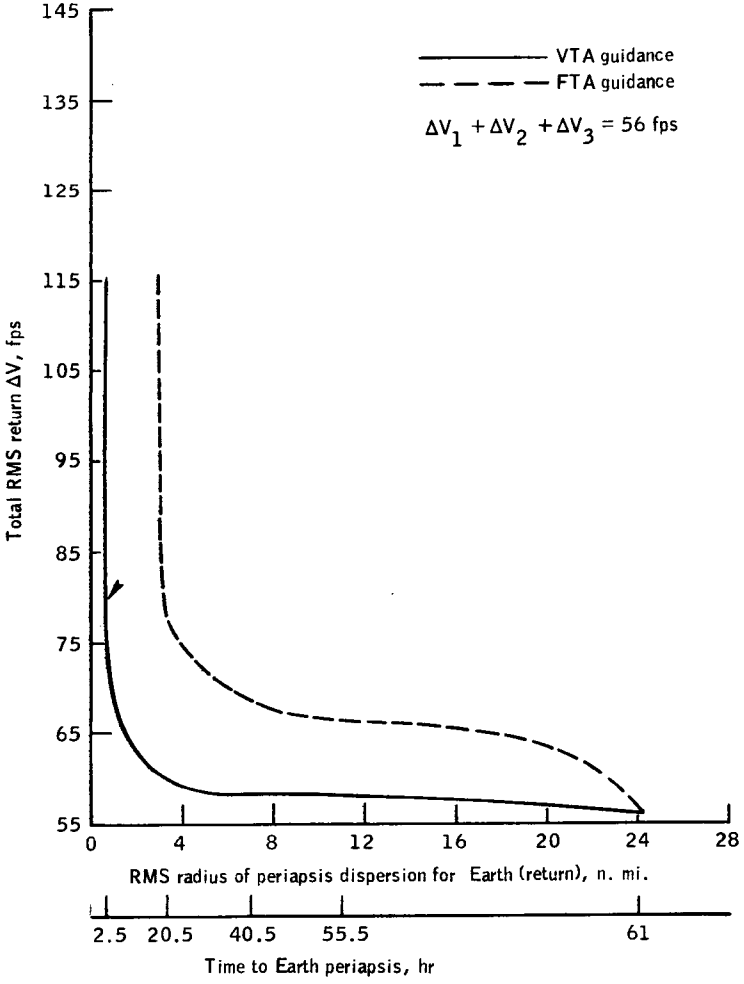

(b) Earth approach phase (return).

Figure 16.- Spacecraft guidance accuracy for 1977 Mars stopover.

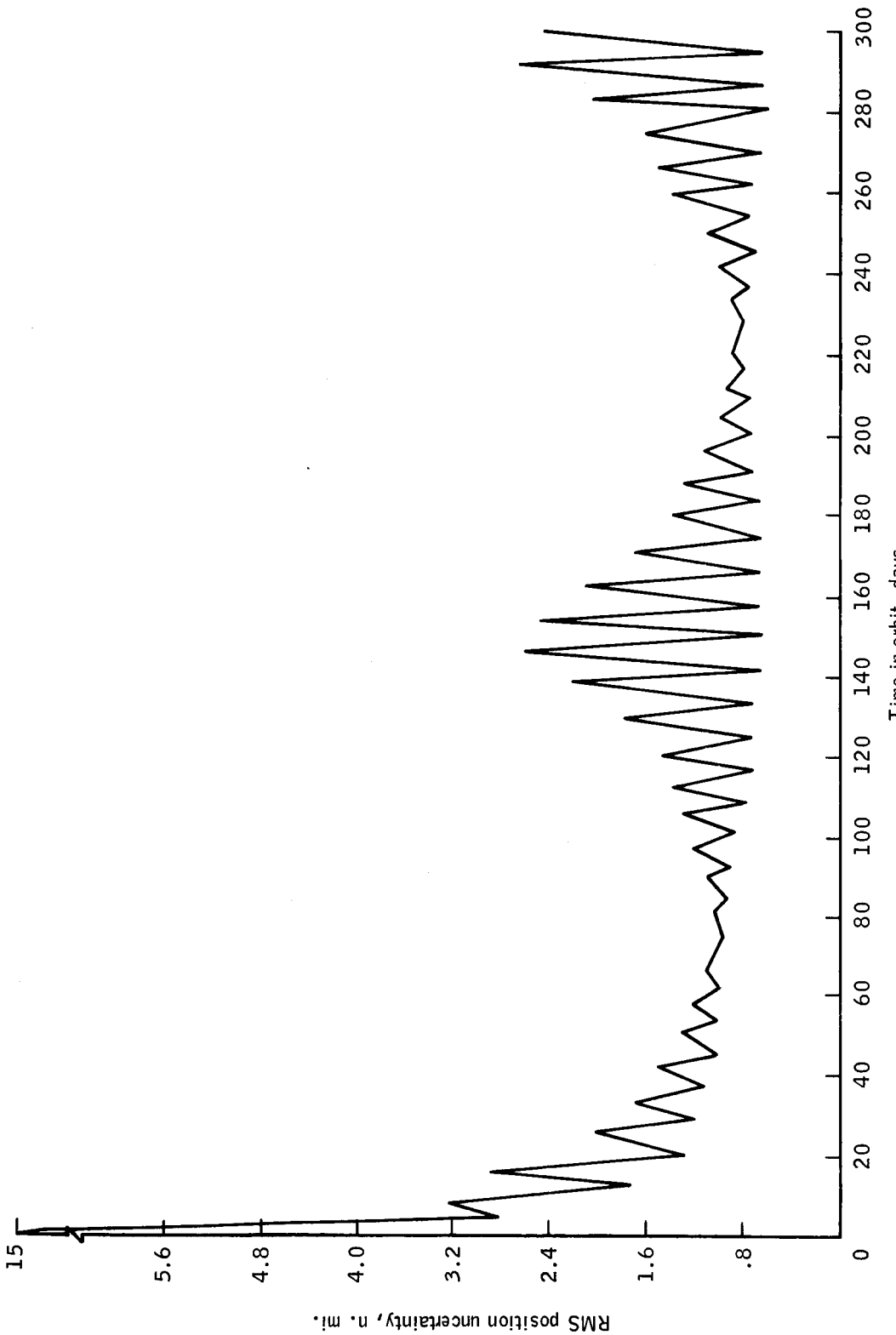

Figure 17.- Orbit navigation accuracy for 1977 Mars stopover.

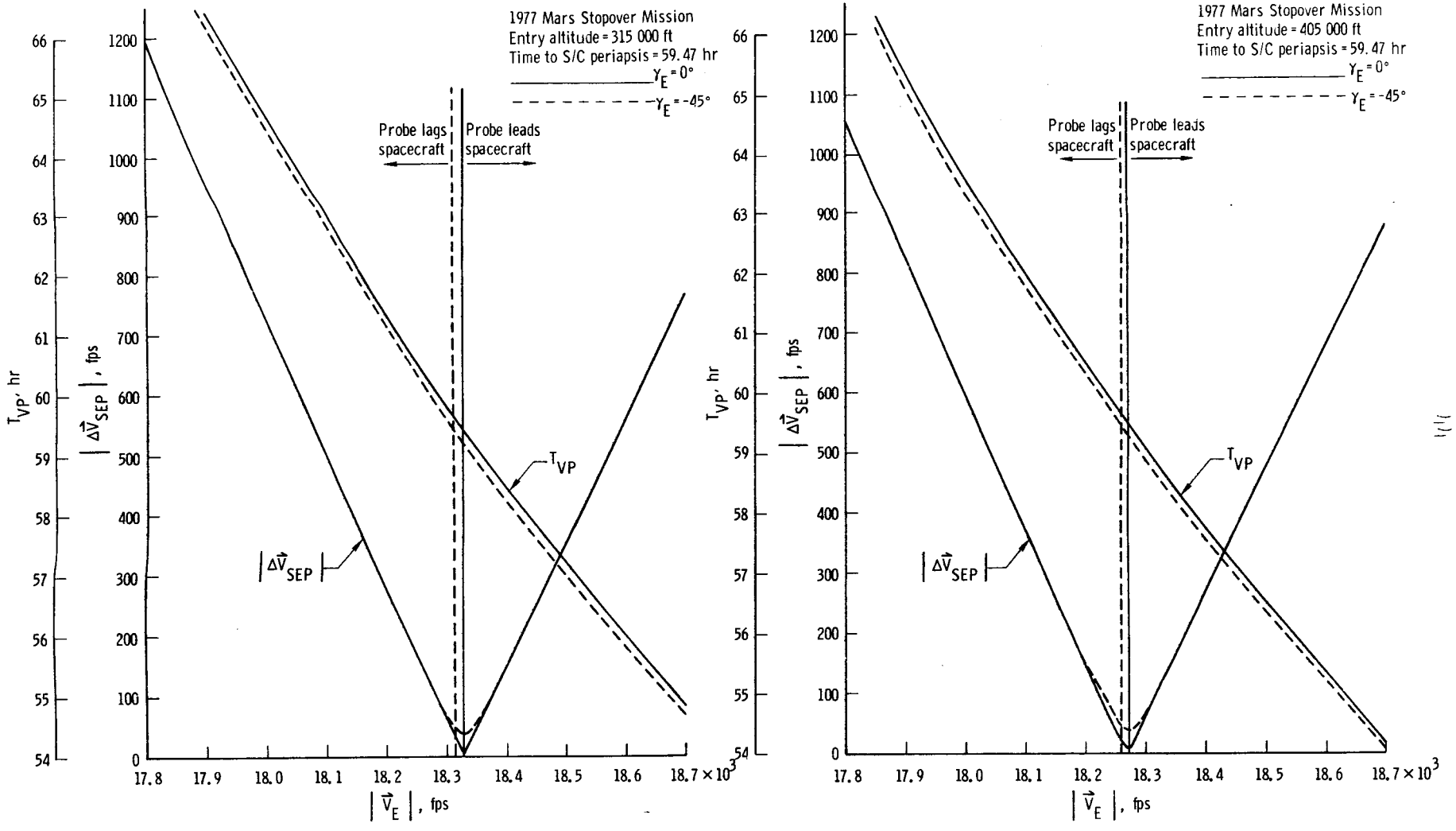

(a) Entry altitude 315 000 ft.

(b) Entry altitude 405 000 ft

Figure 18. - Unmanned probe entry parameters as a function of separation velocity for 1977 Mars stopover.

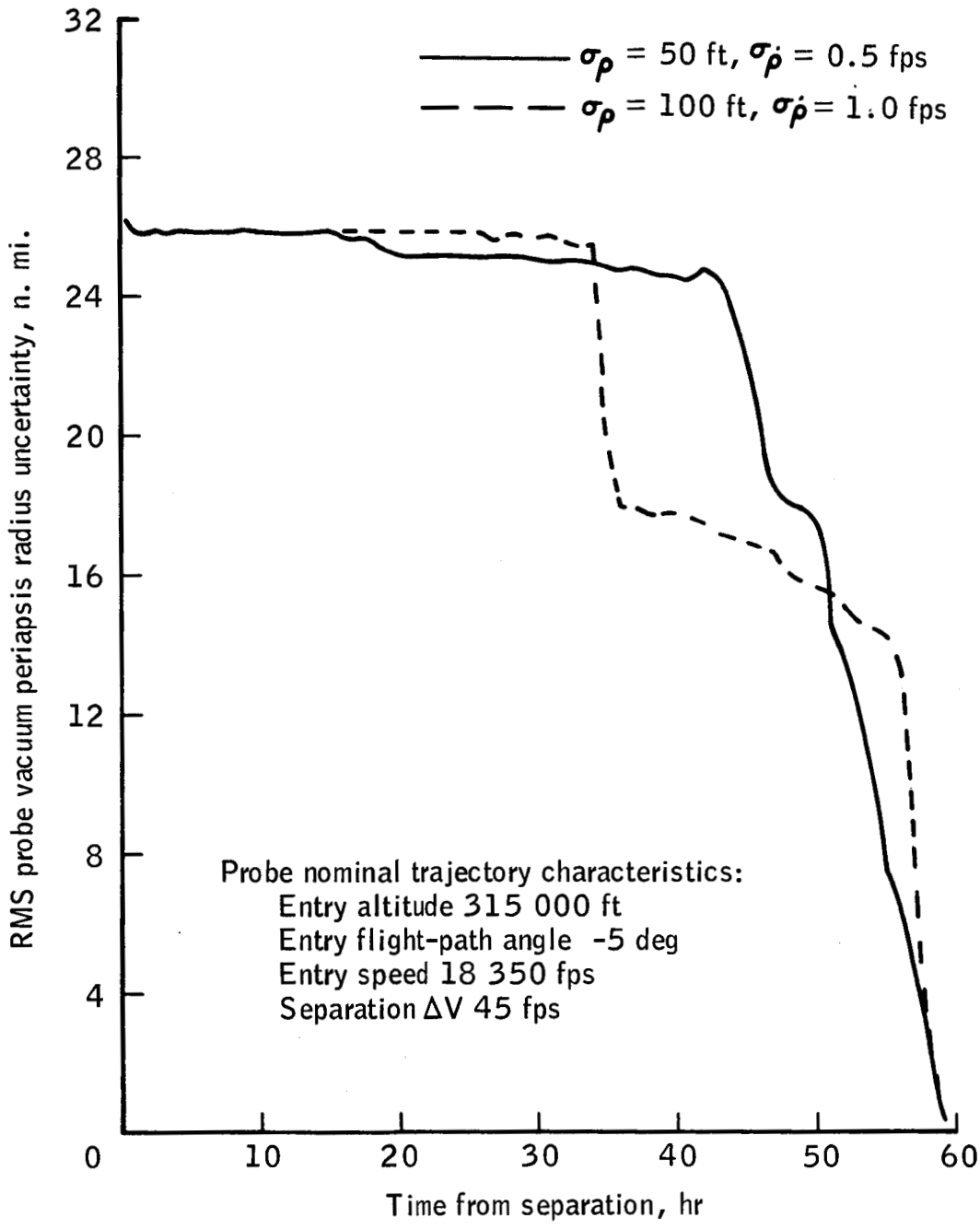

Figure 19.- Probe navigation data for 1977 Mars stop over.

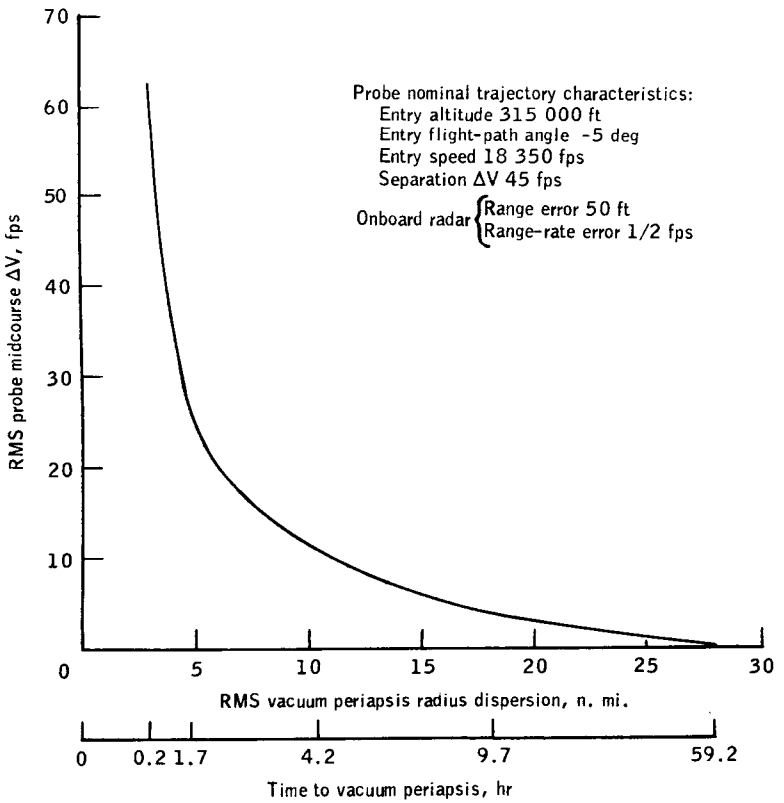

(a) Nominal onboard radar errors.

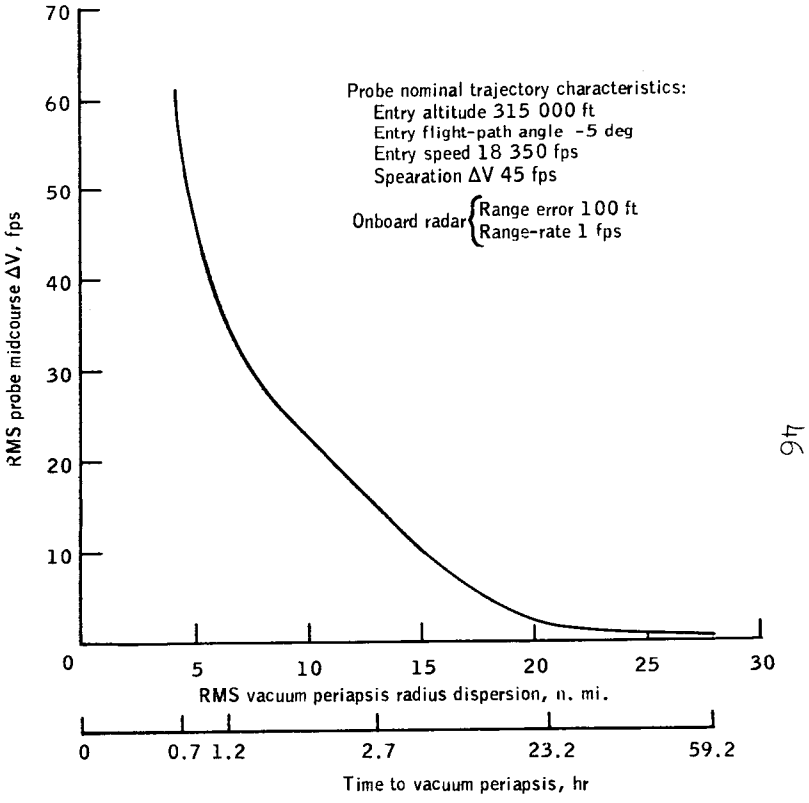

(b) 2X nominal onboard radar errors.

Figure 20.- Probe guidance data for 1977 Mars stopover.

APPENDIX A

PROBE-SPACECRAFT NAVIGATION SYSTEM EQUATIONS

APPENDIX A

PROBE-SPACECRAFT NAVIGATION SYSTEM EQUATIONS

The probe-spacecraft tracking geometry is illustrated in figure A-1. For this study it was assumed that the spacecraft onboard radar measured relative range and range-rate to the probe and simultaneously used an onboard optical sensor, i.e., sextant, to measure the included angle between the target planet horizon and a star. This procedure seems feasible since the onboard **radar** can track the probe continuously and when the spacecraft horizon-star measurement is fed into the onboard computer a command is automatically set up in the navigation program which calls for simultaneous data processing of the radar range and range-rate information.

The data can be processed in the onboard computer using an augmented Kalman filter (ref. 9 and 10). The structure of the augmented filter equations is identical to the standard Kalman filter equations except the state vector dimensions are increased. For this study, the state vector is 12-dimensional and includes the spacecraft and probe positions and velocities. The equation which relates deviations in this state vector at time, t, to deviations at time, t_o, is

$$\begin{bmatrix} \delta\bar{r}_s(t) \\ \delta\bar{V}_s(t) \\ \delta\bar{r}_p(t) \\ \delta\bar{V}_p(t) \end{bmatrix} = \begin{bmatrix} \Phi(t,t_o) & 0 \\ 0 & \Gamma(t,t_o) \end{bmatrix} \begin{bmatrix} \delta\bar{r}_s(t_o) \\ \delta\bar{V}_s(t_o) \\ \delta\bar{r}_p(t_o) \\ \delta\bar{V}_p(t_o) \end{bmatrix} \tag{A1}$$

where $\Phi(t,t_o)$ and $\Gamma(t,t_o)$ are the 6×6 spacecraft and probe state transition matrices, respectively. Define

$$\bar{\xi}(t) = \begin{bmatrix} \delta\bar{r}_s(t) \\ \delta\bar{V}_s(t) \\ \delta\bar{r}_p(t) \\ \delta\bar{V}_p(t) \end{bmatrix} \tag{A2}$$

and

$$\Theta(t,t_o) = \begin{bmatrix} \Phi(t,t_o) & 0 \\ - & \\ 0 & \Gamma(t,t_o) \end{bmatrix} . \qquad (A3)$$

Then equation (A1) becomes

$$\bar{\xi}(t) = \Theta(t,t_o)\bar{\xi}(t_o) \qquad (A4)$$

The initial 12 × 12 covariance matrix for the augmented system, i.e., at probe-spacecraft separation, is defined by

$$P(t_{SEP}) = \begin{bmatrix} E_s(t_{SEP}) & 0 \\ 0 & E_p(t_{SEP}) \end{bmatrix} \qquad (A5)$$

where $E_s(t_{SEP})$ is the spacecraft uncertainty covariance matrix and $E_p(t_{SEP}) = E_s(t_{SEP}) + \Delta E(t_{SEP})$. The term $\Delta E(t_{SEP})$ is the degradation to the probe uncertainty matrix as a result of an imperfect separation maneuver. The equation for propagating the augmented covariance matrix between measurements is given by the equation

$$P(t) = \Theta(t,t_o)P(t_o)\Theta^T(t,t_o) . \qquad (A6)$$

The equation which relates deviations in the observables to state vector deviations is

$$\begin{bmatrix} \delta\beta(t) \\ \delta\rho(t) \\ \delta\dot{\rho}(t) \end{bmatrix} = H(t)\bar{\xi}(t), \qquad (A7)$$

where the 3 × 12 matrix $H(t)$ is written in partitioned form as

$$H(t) = \begin{bmatrix} A(t) & 0 \\ -B(t) & B(t) \end{bmatrix} . \qquad (A8)$$

The 1×6 vector $A(t)$ is defined by

$$A(t) = \begin{bmatrix} \frac{\partial \beta}{\partial \bar{r}_s} & \frac{\partial \beta}{\partial \bar{V}_s} \end{bmatrix} , \tag{A9}$$

and the 2×6 matrix $B(t)$ is defined by

$$B(t) = \begin{bmatrix} \frac{\partial \rho}{\partial \bar{\rho}} & \frac{\partial \rho}{\partial \bar{V}_\rho} \\ \frac{\partial \dot{\rho}}{\partial \bar{\rho}} & \frac{\partial \dot{\rho}}{\partial \bar{V}_\rho} \end{bmatrix} . \tag{A10}$$

The partial derivatives required in equations (A9) and (A10) can be calculated from the following relationships (see fig. A-1).

$$\left.\begin{aligned} \frac{\partial \beta}{\partial \bar{r}_s} &= \frac{r_B}{r_s^3 \cos\theta}\bar{r}_s + \frac{\bar{r}_s \times (\bar{r}_s \times \hat{u}_s)}{r_s^2 |\bar{r}_s \times \hat{u}_s|} \\ \frac{\partial \beta}{\partial \bar{V}_s} &= 0 \end{aligned}\right\} \tag{A11}$$

$$\left.\begin{aligned} \frac{\partial \rho}{\partial \bar{\rho}} &= \frac{\bar{\rho}^T}{\rho} \\ \frac{\partial \rho}{\partial \bar{V}_\rho} &= 0 \\ \frac{\partial \dot{\rho}}{\partial \bar{\rho}} &= \frac{\bar{V}_\rho^T}{\rho}\left[I - \frac{\bar{\rho}\bar{\rho}^T}{\rho^2}\right] \\ \frac{\partial \dot{\rho}}{\partial \bar{V}_\rho} &= \frac{\bar{\rho}^T}{\rho} \end{aligned}\right\} \tag{A12}$$

The equations required to update the augmented uncertainty matrix, P(t), at the time of a measurement can now be written

$$\left.\begin{aligned} P^{+}(t) &= [I - K(t)H(t)]P^{-}(t) \\ K(t) &= P^{-}(t)H^{T}(t)M^{-1}(t) \\ M(t) &= H(t)P^{-}(t)H^{T}(t) + R(t) \end{aligned}\right\} \qquad \text{(A13)}$$

where the 3 × 3 covariance matrix of measurement errors, R(t), is defined by

$$R(t) = \begin{bmatrix} \sigma_{\beta}^{2} & 0 & 0 \\ 0 & \sigma_{\rho}^{2} & 0 \\ 0 & 0 & \sigma_{\dot{\rho}}^{2} \end{bmatrix}, \qquad \text{(A14)}$$

and the (-) and (+) superscripts refer to a quantity before and after the measurement, respectively.

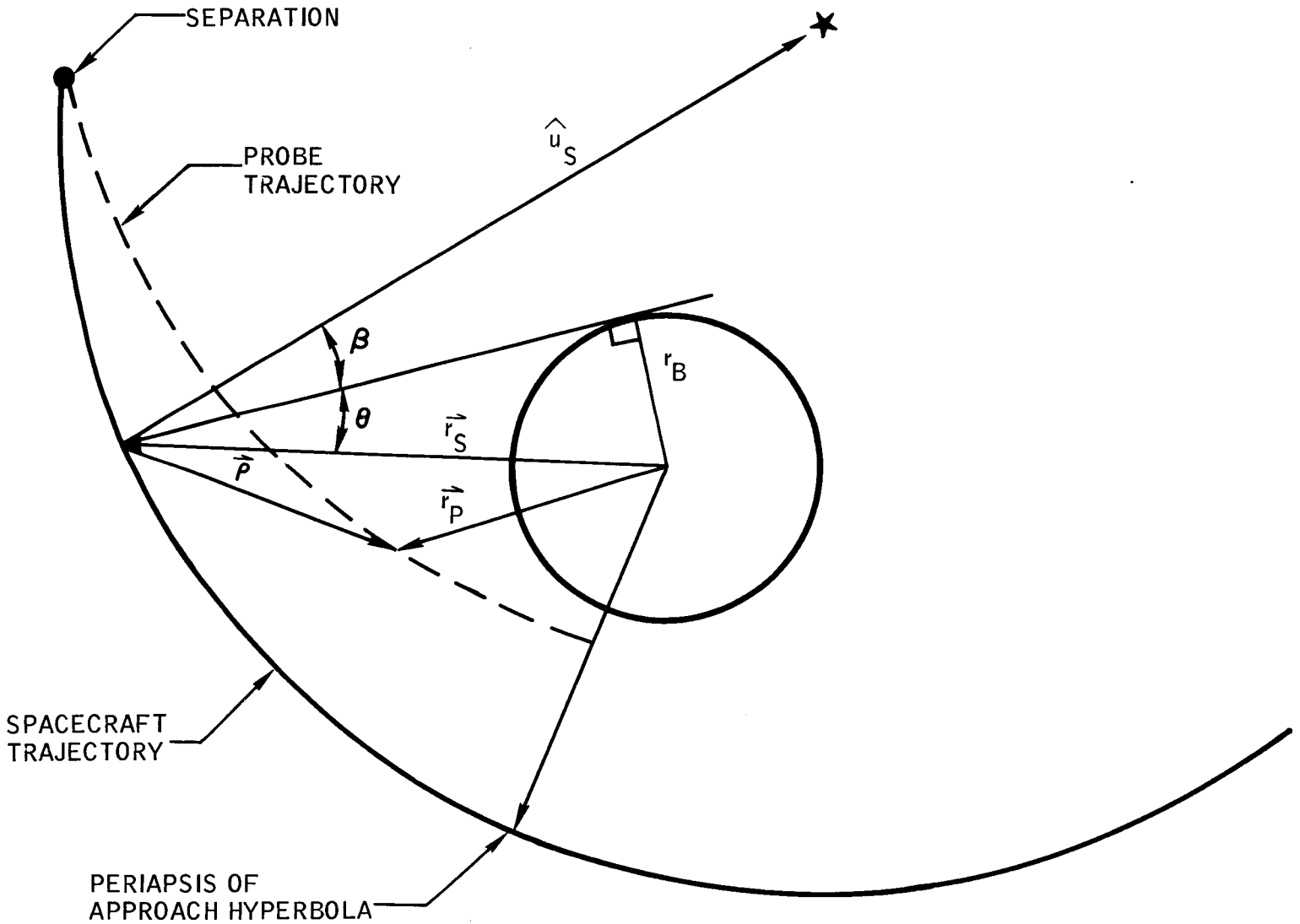

Figure A-1.- Probe-spacecraft tracking geometry.

REFERENCES

1. Cicolani, Luigi S.: Interplanetary Midcourse Guidance Using Radar Tracking and On-Board Observation Data. NASA TN D-3623, 1966.

2. White, John S.; Callas, George P.; and Cicolani, Luigi S.: Application of Statistical Filter Theory to the Interplanetary Navigation and Guidance Problem. NASA TN D-2697, 1965.

3. Murtagh, Thomas B.; Lowes, Flora B.; and Bond, Victor R.: Navigation and Guidance Analysis of a Mars Probe Launched From a Manned Flyby Spacecraft (NASA TN to be published).

4. Bond, Victor R.: Matched Conic Solutions to Interplanetary Trajectory Problems that Insure State Vector Continuity at all Boundaries. (NASA TN to be published).

5. Thibodeau, Joseph R.: Use of Planetary Oblateness for Parking Orbit Alignment. (NASA TN to be published).

6. Battin, Richard H.: Astronautical Guidance. McGraw-Hill Book Company, Inc., 1964.

7. Rohde, Paul J.: The Scheduling of Measurements for Analysis of an Onboard Navigation System. Philco WDL-TR2600 Prepared for Marshall Space Flight Center under Contract No. NAS 8-11198, 1965.

8. Baker, D. S.; Sears, N. E.; and White, R. L.: Lunar Orbit Navigation Performance With Various Random and Systematic Errors. MIT Instrumentation Laboratory Report E-1983, 1966.

9. Suddath, J. H.; and Carney, T. M.: Semi-Coupled Filters With Application to the Rendezvous of Space Vehicles. Presented at the Institute of Navigation Meeting in Houston, Texas, April 29-30, 1965.

10. Murtagh, Thomas B.: Analysis of Sextant Navigation Measurements During Lunar Module Rendezvous. NASA TN D-3873, 1967.